# Highly dispersive magnons with spin-gap-like features in the frustrated ferromagnetic $S = \frac{1}{2}$ chain compound $Ca_2Y_2Cu_5O_{10}$ detected by inelastic neutron scattering

M. Matsuda,[1] J. Ma,[1,*] V. O. Garlea,[1] T. Ito,[2] H. Yamaguchi,[2] K. Oka,[2] S.-L. Drechsler,[3] R. Yadav,[3] L. Hozoi,[3] H. Rosner,[4] R. Schumann,[5] R. O. Kuzian,[6,7] and S. Nishimoto[3,8]

[1]*Neutron Scattering Division, Oak Ridge National Laboratory, Oak Ridge, Tennessee 37831, USA*
[2]*National Institute of Advanced Industrial Science and Technology (AIST), Tsukuba, Ibaraki 305-8562, Japan*
[3]*Institute of Theoretical Solid State Physics, IFW Dresden, Helmholtzstraße 20, D-01069 Dresden, Germany*
[4]*Max-Planck-Institute of Chemical Physics, Nöthnitzer Str. 40, D-01187 Dresden, Germany*
[5]*Department of Physics, Institute of Theoretical Physics, TU Dresden, D-1062 Dresden, Zellescher Weg 17, Germany*
[6]*Institute for Problems of Materials Science, NASU, Krzhizhanovskogo 3, 03180 Kiev, Ukraine*
[7]*Donostia International Physics Center (DIPC), Paseo Manuel de Lardizabal 4, San Sebastian/Donostia, 20018 Basque Country, Spain*
[8]*Department of Physics, Institute of Theoretical Physics, TU Dresden, Mommsenstraße, D-01069 Dresden, Germany*

(Received 11 June 2018; revised manuscript received 13 August 2019; published 12 September 2019)

We report inelastic neutron scattering experiments in $Ca_2Y_2Cu_5O_{10}$ and map out the full one-magnon dispersion which extends up to a record value of 53 meV for frustrated ferromagnetic (FM) edge-sharing $CuO_2$ chain (FFESC) cuprates. A homogeneous spin-1/2 chain model with a FM nearest-neighbor (NN), an antiferromagnetic (AFM) next-nearest-neighbor (NNN) inchain, and two diagonal AFM interchain couplings (ICs) analyzed within linear spin-wave theory (LSWT) reproduces well the observed strong dispersion along the chains and a weak one perpendicularly. The ratio $\alpha = |J_{a2}/J_{a1}|$ of the FM NN and the AFM NNN couplings is found as ~0.23, close to the critical point $\alpha_c = 1/4$ which separates ferromagnetically and antiferromagnetically correlated spiral magnetic ground states in single chains, whereas $\alpha_c > 0.25$ for coupled chains is considerably upshifted even for relatively weak IC. Although the measured dispersion can be described by homogeneous LSWT, the scattering intensity appears to be considerably reduced at ~11.5 and ~28 meV. The gaplike feature at 11.5 meV is attributed to magnon-phonon coupling whereas based on density matrix renormalization group simulations of the dynamical structure factor the gap at 28 meV is considered to stem partly from quantum effects due to the AFM IC. Another contribution to that gap is ascribed to the intrinsic superstructure from the distorting incommensurate pattern of CaY cationic chains adjacent to the $CuO_2$ ones. It gives rise to nonequivalent $CuO_4$ units and Cu-O-Cu bond angles $\Phi$ and a resulting distribution of all exchange integrals. The $J$'s fitted by homogeneous LSWT are regarded as average values. The record value of the FM NN integral $J_1 = 24$ meV among FFESC cuprates can be explained by a *nonuniversal* $\Phi(\neq 90^\circ)$ and Cu-O bond length dependent *anisotropic* mean direct FM Cu-O exchange $\bar{K}_{pd} \sim 120$ meV, similar to a value of 105 meV for $Li_2CuO_2$, in accord with larger values for $La_2CuO_4$ and $CuGeO_3$ (~110 meV) reported by Braden *et al.* [Phys. Rev. B **54**, 1105 (1996)] phenomenologically. Enhanced $K_{pd}$ values are also needed to compensate a significant AFM $J_{dd} \geqslant 6$ meV from the $dd$ channel, generic for FFESC cuprates but ignored so far.

DOI: 10.1103/PhysRevB.100.104415

## I. INTRODUCTION

One-dimensional (1D) antiferromagnetic (AFM) spin ($S$) 1/2 systems have been studied intensively, since they exhibit exotic quantum effects. The spinon is a typical feature generic for the AFM Heisenberg chain. In contrast, 1D ferromagnetic (FM) systems do not show pronounced quantum effects since the FM state is an eigenstate of the spin Hamiltonian. However, frustrating couplings, such as a next-nearest neighbor (NNN) AFM $J_2$ and/or AFM interchain couplings (ICs), can cause a more interesting ground state [1]. In particular, they may induce gaps of different nature for excited states, strongly dependent on the sign of the nearest-neighbor (NN) exchange $J_1$: well known for AFM $J_1$ for $0.241 \leqslant \alpha \lesssim 0.7$ in the context of the spin-Peierls problem [2] and recently found for FM $J_1$ at $\alpha > \alpha_c(=1/4)$ due to quantum fluctuations [3], where the frustration $\alpha$ reads

$$\alpha = J_2/|J_1|. \tag{1}$$

In $Ca_2Y_2Cu_5O_{10}$ (CYCO) and any other edge-sharing chain cuprates (see Sec. II and Fig. 1) described by the $S = 1/2J_1$-$J_2$ model, $J_2 > 0$ always holds due to the Cu-O-O-Cu superexchange. Then $\alpha^{-1}$ measures the coupling of two interpenetrating ferromagnetically interacting AFM Heisenberg chains, where the $J_1$-$J_2$ chain is regarded as a topologically equivalent zigzag chain with different NN couplings. For FM $J_1$, the ground state changes from a FM to an AFM spin liquid

[*]Present address: Department of Physics and Astronomy, Shanghai Jiao Tong University, Shanghai 200240, People's Republic of China.

 

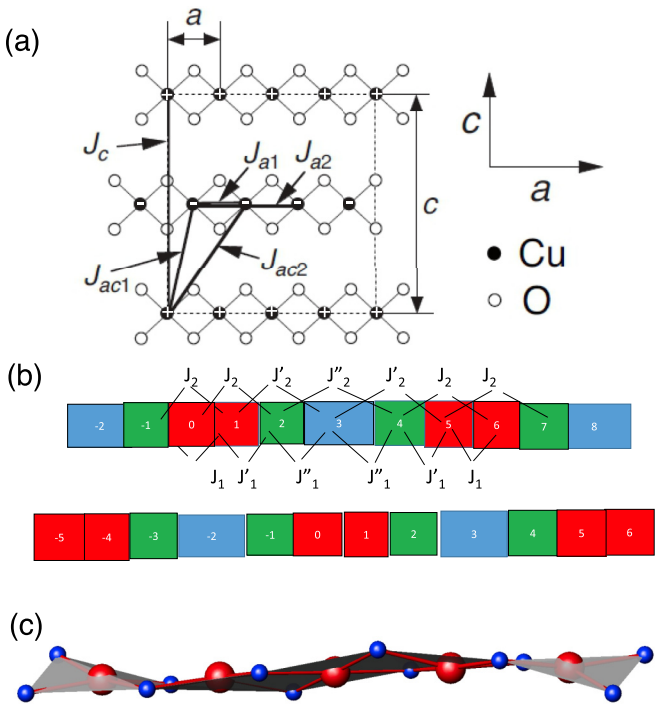


FIG. 1. (a) Schematic view of the $CuO_2$ spin chains in the *ac* plane of $Ca_2R_2Cu_5O_{10}$ ($R$ = Y and Nd) for an averaged idealized structure. Inchain couplings $J_{a1}$ and $J_{a2}$ as well as the two diagonal NN and NNN ICs $J_{ac1}$, $J_{ac2}$, and $J_c$ are shown. The spin order in the *ac* plane is also depicted. Spins along $+b$ ($-b$) directions are shown with "+" ("−"), respectively. (b) A nonideal $Cu_5O_{10}$ chain due to its misfit with the adjacent cationic $Ca_2R_2$ ($R$ = Nd and Y) chains adopting symmetric distortions for simplicity. The three nonequivalent $CuO_4$ plaquettes of this case are depicted by red, green, and blue rectangles. Here a chain has three different boundaries (red-red, red-green, and red-blue pairs of bridging O) and three different Cu-O-Cu bond angles, giving rise to three different AFM contributions to each NN coupling (see Sec. V). At least three different NN and NNN couplings denoted by $J_1$, $J'_1$, and $J''_1$ as well as $J_2$, $J'_2$, and $J''_2$ [instead of two single $J_{a1}$ and $J_{a2}$ shown in panel (a)] appear. The general asymmetric chain has five nonequivalent plaquettes and a couple of five NN and NNN inchain couplings, respectively. (c) A distorted single chain according to the model by Thar *et al.* [8] (view along the *c* axis). Red (blue) spheres denote Cu (O) ions.

with noncollinear spiral fluctuations for $\alpha > \alpha_c$ [1]. There are only few materials with long edge-sharing $CuO_2$ chains and relatively large $J_1$ and $J_2$ values near such a critical point. We mention three of them: (i) $Li_2CuO_2$ (LICO), with FM inchain order below its Néel temperature $T_N \approx 9$ K; (ii) $Li_2ZrCuO_4$, with a spiral ordering with $\alpha \approx 0.33$ (at $T < 7$ K), predicted in Ref. [4] and confirmed in Refs. [5,6] (see also Ref. [7]); and (iii) further candidates near quantum criticality, where the insight gained for CYCO might be helpful to elucidate their exchange interactions and unusual magnetic states. Among them are $La_6Ca_8Cu_{24}O_{41}$ and derivatives which contain besides two-leg spin ladders (TLLs) similar frustrated FM edge-sharing $CuO_2$ chains (FFESCs).

A recent inelastic neutron-scattering (INS) study for LICO [9–11] revealed a relatively large $J_1 = -19.7$ meV, $\alpha = 0.332$, and a weak but nevertheless decisive AFM IC of 0.78 meV. Although $\alpha > \alpha_c$, a FM arrangement is realized in the chains due to specific AFM ICs. Within a refined linear spin-wave analysis employing the full magnon dispersion up to 53 meV and performing measurements along those scattering directions where the small IC can be separated from the large inchain one, we will show that $J_1$ of CYCO well exceeds the largest $J_1$ values reported so far for LICO [9] and $Li_2ZrCuO_4$ [4,5] among the FFESC family.

As shown in detail below, CYCO with a FM stacking of 2D Néel planes along the *b* axis is the "2D analogon" of LICO. CYCO has the highest $T_N = 29.5$ K [12–14] and together with LICO the largest ordered magnetic moments among all FFESC. The critical point for the system of antiferromagnetically coupled mutually shifted NN chains by half a Cu-Cu distance in the chain direction (Fig. 1) is *upshifted* to $\alpha > 1/4$, reflecting a stabilization of the FM inchain ordering. On the other hand, the spin-wave dispersion for LICO shows a flat minimum at the magnetic zone center, which reflects also incommensurate correlations along the chains. Here weak AFM O-mediated ICs between adjacent chains are relevant too [9–11].

Since the large FM $J_1$ is the origin for a large magnon dispersion, its microscopic origin is of interest for the cuprate physics in general to be addressed in the framework of multiband Cu-O *pd* models. Then $J_1$ depends first of all on the direct FM exchange $K_{pd}$ between two holes on NN Cu and O sites and on Hund's exchange $J_H$ of two holes in two different O $2p$ orbitals on the same O site which bridges twice two NN Cu sites. Although being key quantities, neither is precisely known. In particular, the $K_{pd} = 50$ meV suggested in Ref. [15] for LICO and CYCO and *all* other FFESC differs by more than 200% from the empirical value for $CuGeO_3$ [2] and even by 400% for the corner-sharing $La_2CuO_4$, where $K_{pd}$ and its weaker NN O-O counterpart, $K_{pp}$, are known from advanced many-body calculations [16,17]. We report on complementary quantum chemical (QC) and density functional theory (DFT) computations for LICO, derive also a significant $K_{pd}$ value and stress its key role for the FM $J_1$ and the magnon dispersion [9,10]. We resolve a long-standing puzzle for seemingly AFM or small FM Curie-Weiss temperatures ($\Theta_{CW}$) [13,18] at odds with the inchain FM alignment of magnetic moments in the Neél state using a high-temperature expansion (HTE) for the spin susceptibility $\chi(T)$ (Sec. V A). In the Supplemental Material [7] we present a rich collection of cuprates with edge-sharing elements, provide further support for sizable FM NN couplings, and explain special reasons for weak or even AM values.

## II. PREVIOUS AND REFINED RESULTS IN CYCO

CYCO consists of edge-sharing $CuO_2$ chains [19], each $[CuO_2]^{-2}$ unit carries a spin 1/2 [20]. The chains in the *ac* plane are shown in Fig. 1(a). CYCO exhibits an AFM order below $T_N = 29.5$ K. The spins align ferromagnetically along the *a* axis (chain direction) and *b* axis and antiferromagnetically along the *c* axis [12,13]. The ordered magnetic moment is $0.9\mu_B$. The magnetic structure in the *ac* plane is shown in Fig. 1(a). CYCO shows commensurate and incommensurate orders of Ca and Y, which gives rise to a supercell with $5 \times a$ and $4.11 \times c$ in the simplest approximation [19]. In

this supercell, there are 4 Ca/Y and 5 Cu positions along the chain. The alternating $Ca^{2+}/Y^{3+}$ chains cause sizable shifts of the O ions [Figs. 1(b) and 1(c)] at variance to chains with equivalent O sites [8]. However, it is unclear how much this superstructure (SS), affecting mostly the O sites, does modify the long-range magnetic order. The inchain spin arrangement is FM and no magnetic SS has been found so far. Hence, the static magnetic order seems to be hardly affected by the chain distortions, probably due to the few O spins.

The spin Hamiltonian for CYCO may be written as

$$\hat{H} = \hat{H}_{ch} + \hat{H}_{IC} + \hat{H}_A, \tag{2}$$

where $\hat{H}_{ch}(\hat{H}_{IC})$ describes in(inter)-chain isotropic Heisenberg interactions of the form

$$\hat{H}_{ch} + \hat{H}_{IC} = \frac{1}{2}\sum_{\mathbf{R},\mathbf{r}} J_{\mathbf{r}} \hat{\mathbf{S}}_{\mathbf{R}} \hat{\mathbf{S}}_{\mathbf{R}+\mathbf{r}}, \tag{3}$$

$J_{\mathbf{r}}$ being exchange interaction between a pair of copper spins $\hat{\mathbf{S}}_{\mathbf{R}}$ and $\hat{\mathbf{S}}_{\mathbf{R}+\mathbf{r}}$ in the same (for $\hat{H}_{ch}$) or in different (for $\hat{H}_{IC}$) chains; $\hat{H}_A$ denotes uniaxial pseudodipolar anisotropic interactions:

$$\hat{H}_A = \frac{1}{2}\sum_{\mathbf{R},\mathbf{r}} D_{\mathbf{r}} \hat{S}^z_{\mathbf{R}} \hat{S}^z_{\mathbf{R}+\mathbf{r}}. \tag{4}$$

In previous works [21–24], the INS results were interpreted assuming that all Cu sites are equivalent, i.e., ignoring a lattice modulation. The magnon dispersion curves were fitted by linear spin-wave theory (LSWT):

$$\begin{aligned}
&\omega_q = \sqrt{A_q^2 - B_q^2}, \quad \text{with} \\
&A_q = J_{a1}(\cos q_a - 1) + J_{a2}(\cos 2q_a - 1) + J_b(\cos q_b - 1) \\
&\quad + J_c(\cos q_c - 1) + 2J_{ab}\left(\cos\frac{q_a}{2}\cos\frac{q_b}{2} - 1\right) \\
&\quad + 2(J_{ac1} + J_{ac2}) - D, \\
&B_q = 2J_{ac1}\cos\frac{q_a}{2}\cos\frac{q_c}{2} + 2J_{ac2}\cos\frac{3q_a}{2}\cos\frac{q_c}{2},
\end{aligned} \tag{5}$$

where $J_{a1}$, $J_{a2}$ are FM NN and AFM NNN in-chain interactions, $J_{ac1}$ and $J_{ac2}$ are NN and NNN ICs in the $ac$ plane (Fig. 1), $J_b$ and $J_c$ are interactions along the $b$ and $c$ directions, respectively; $\mathbf{q} = (q_a, q_b, q_c) = 2\pi(h, k, l)$ is the magnon momentum. Only an averaged value $D$ of the anisotropy parameters $D_{\mathbf{r}_1}, D_{\mathbf{r}_2}$ enters the dispersion

$$D = \sum_{\mathbf{r}_1} D_{\mathbf{r}_1} - \sum_{\mathbf{r}_2} D_{\mathbf{r}_2}, \tag{6}$$

where the vectors $\mathbf{r}_1(\mathbf{r}_2)$ connect sites of the same (different) AFM sublattice.

Let us recall that a FM state is an eigenstate of $\hat{H}_{ch} + \hat{H}_A$ and magnons are its *exact* one-particle excitations. That is why the ordered moment in CYCO is close to 1 $\mu_B$ and LSWT provides adequate values of exchange parameters (cf. Sec. V C 1). The only source of quantum fluctuations in CYCO is the relatively weak $\hat{H}_{IC}$. It affects the magnon dynamics but does not change the overall shape of the LSWT dispersion, Eq. (5) (see Sec. V A).

In Ref. [21] the dispersion along high-symmetry directions starting from the zone center Γ was measured up to $W_E \sim$ 10 meV. The full dispersion curves were available for the $b$ and $c$ directions, $(0, k, 0)$ and $(0, 0, l)$, respectively, thus the IC parameters $J_b = 0.06$, $J_{ab} = 0.03$, $J_c = 0$, and $J_s = J_{ac1} + J_{ac2} \approx 2.24$ meV were established. On the contrary, only a small part of the dispersion was possible to be measured along the chain direction $a$. Inspection of Eq. (5) shows that the dispersion along the line $(h, 0, 0)$ is affected by the ICs. The influence of the tiny $J_{ab}$ can be ignored but $J_{ac1,2}$ do substantially affect the dispersion at small $\mathbf{q}$. Moreover, the dispersion depends not only on the sum $J_s$ but also on the ratio $J_{ac1}/J_{ac2}$. That is why the fit of those measurements was ambiguous. Table I shows how the extracted inchain couplings became more and more accurate by including data up to higher energies.

TABLE I. The inchain couplings $J_{a1}$ and $J_{a2}$ from INS data analyzed within LSWT, the maximum energy ($W_E$) below which the INS data were fitted, and $\alpha = |J_{a2}/J_{a1}|$. Values in the first row represents theoretical predictions from Ref. [15].

| Year | $J_{a1}$ (meV) | $J_{a2}$ (meV) | $W_E$ (meV) | $\alpha$ | Ref. |
|---|---|---|---|---|---|
| 1998 | −2.2 | 4.7 | – | 2.2 | [15] |
| 2001 | −8 | 0.4 | 10 | 0.05 | [21] |
| | −6.9 | 0.0 | 10 | 0 | [21] |
| 2012 | −19.6 | 3.7 | 25 | 0.19 | [24] |
| 2019 | −24 | 5.5 | 53 | 0.23 | Present work |

Measurements along the lines $(h, 0, 1.25)$ and $(h, 0, 1.5)$ were first performed in Ref. [24]. The dispersion along the line $(h, 0, 1.5)$ $(q_c = 3\pi)$ is independent of $J_{ac1,2}$, and its curvature near $h = 0$ is determined by $\alpha$. It reveals a substantial value of $J_{a2}$ and allows a new fit that includes also broad excitation data up to 25 meV. Both $J_{a1}$ and $J_{a2}$ (fourth row of Table I) were found to be much stronger and consistent with theory. As mentioned above, for $\alpha > 1/4$, the ground state is an AFM spiral state. In our previous study [24] we found $\alpha \sim 0.19$, below the critical value of a single chain. In order to determine the overall profile of the magnon dispersion and refine also $\alpha$, we performed INS experiments using a time-of-flight chopper spectrometer. This way, we probed the full dispersion that extends up to ∼53 meV and $\alpha$ was refined as ∼0.23, closer to $\alpha_c$.

As previously observed [21], the intensity of the magnons appears to be reduced at ∼11.5 meV. In addition to this, we also found another gaplike behavior at ∼28 meV. We refine the exchange parameters and discuss the origin of the gaplike behavior in the magnon dispersion. The gap at ∼11.5 meV is related to the coupling with a weakly dispersive optical phonon. The gaplike feature at ∼28 meV is ascribed to quantum effects due to the AFM ICs [21] and to the SS mentioned above.

## III. EXPERIMENTAL METHOD

A CYCO single crystal was grown by the traveling solvent floating zone (TSFZ) method in air. The dimensions of the rod shaped crystal was ∼6Φ × 25 $mm^3$. This crystal was already used in previous INS studies [21–24]. The present INS experiments were carried out on a hybrid neutron spectrometer HYSPEC [25] installed at the Spallation Neutron

Source (SNS) and a triple-axis spectrometer HB-1 installed at the High Flux Isotope Reactor (HFIR) at Oak Ridge National Laboratory (ORNL). We utilized two incident energies of 27 and 60 meV on HYSPEC. Energy resolutions at the elastic position are ∼1.3 and ∼3.8 meV with $E_i = 27$ and 60 meV, respectively. Neutrons with a final energy of 13.5 meV were used, together with a horizontal collimator sequence of 48′–80′–S–80′–240′ on HB-1. The energy resolution at the elastic position amounts to ∼1.4 meV. Contamination from higher-order beams was effectively eliminated using pyrolytic graphite filters. The single crystal was oriented in the $(H, K, 0)$ scattering plane and mounted in a closed-cycle $^4$He gas refrigerator on HYSPEC. On HB-1, the single crystal was oriented in the $(H, K, 0)$ and $(H, 0, L)$ scattering planes and mounted in a closed-cycle $^4$He gas refrigerator. The visualization of the HYSPEC data were performed using the DAVE software [26].

## IV. EXPERIMENTAL RESULTS AND SPIN WAVES

### A. Interchain couplings (ICs)

As mentioned above, the previously studied dispersion along the $(0, 0, l)$ direction provides only the sum of ICs in the *ac* plane $J_s = J_{ac1} + J_{ac2} \approx 2.24$ meV and the anisotropy parameter $D = -0.45$ meV [24]. As pointed out in Ref. [24], the weak ICs can be fitted more accurately from the dispersion relations at $(h, k, l)$ with $h \neq 0$ and any $k$ value, where the inchain couplings do not contribute. Hence, we probed the magnon at $(h, 0, l)$ with $h = 0$, 0.025, 0.005, and 0.1 at $T = 5.5$ K on HB-1. Its dispersion is shown in Fig. 2. The LSWT analysis yields a much larger NNN IC on the two adjacent chains $J_{ac2} = 2.26$ meV than the NN counterpart $J_{ac1} = 0.12$ meV (cf. the ratio $\tilde{J}_1/\tilde{J}_2 \sim 0.1$ in LICO [9]). The average anisotropic exchange parameter $D$ in Eq. (6) was found as −0.21 meV.

Analyzing the unusual intensity suppression near 30 meV with the aid of density matrix renormalization group calculations (see Sec. V A), we find that the ICs would most effectively suppress the intensity when $J_{ac1} \gg J_{ac2}$. This points to the imaginary part of the magnon self-energy $\Im\Sigma$, ignored in LSWT. It might cause this different behavior while $\Re\Sigma$, which governs the dispersion, is less sensitive to the ratio $J_{ac1}/J_{ac2}$.

An almost flat dispersion along the $b$ axis is reproduced [Fig. 2(b)] with the same coupling values as in our previous work [21,23,24]. The difference of the anisotropy parameter $D_b$ from $D$ was explained in Ref. [21] by a small deviation of the spin-Hamiltonian's anisotropy from uniaxial symmetry; the deviation does not visibly split the spin wave branches in the *ac* plane and is not considered here. We mention the couplings as a useful reference for a realistic estimate of the analogous "face-to-face" interaction of $CuO_4$ plaquettes along the $a$ axis in LICO in view of its role in the FM alignment of magnetic moments along the chains under debate [11,27] and an order by disorder scenario [28] versus the AFM IC mechanism based on shifted adjacent chains in Refs. [9,29,30]. To resolve this problem experiments around $\alpha_c$ would be helpful. In particular, an INS study under pressure and an analysis like ours would be interesting in view of the pressure study of LICO [31,32], where above 6 GPa a phase transition to a monoclinic FM phase has been detected. Due to the larger IC coupling in CYCO higher pressures might be necessary for a similar transition. Hence, studies in $La_6Ca_8Cu_{24}O_{41}$ might be easier to perform, although any analysis of the dispersive magnon modes could be difficult due to the presence of ladder spinons. In any event, pressure is a promising tool (see also the estimate of $J_1$ and $\alpha$ in Sec. E of the Supplemental Material [7]).

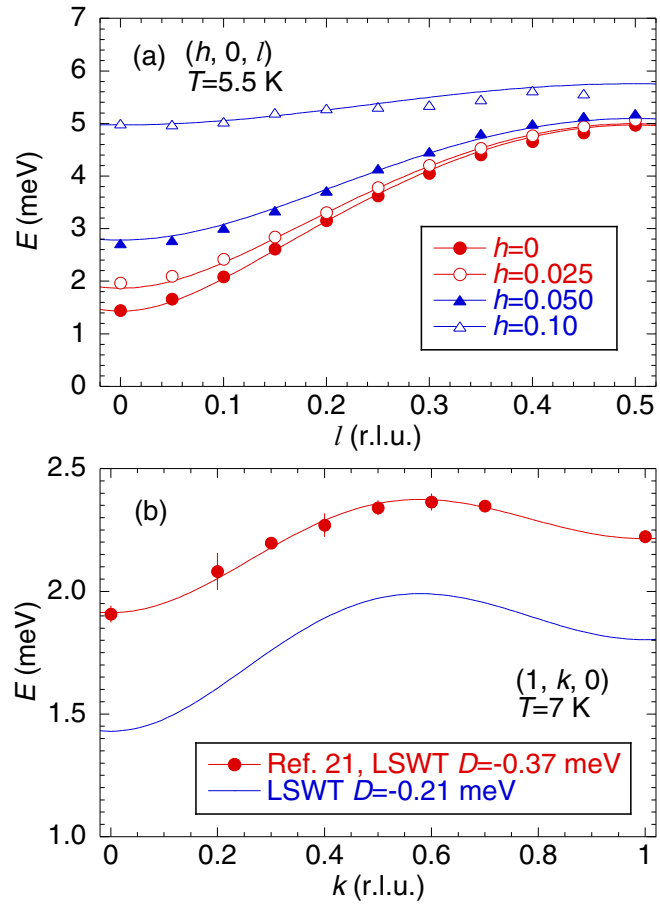


FIG. 2. (a) The weak magnon dispersion of CYCO perpendicular to the chain ($a$ axis) direction within the *ac* plane [$(h, 0, l)$ with $h = 0$, 0.025, 0.005, and 0.1], measured at $T = 5.5$ K with $E_f = 13.5$ meV. Solid curves: the dispersions calculated using LSWT with the two skew ICs $J_{ac1} = 0.12$, $J_{ac2} = 2.26$, and the anisotropy parameter $D = -0.21$ meV. The error bars are smaller than the size of the symbols. (b) The dispersion along the $b$ axis, which is well reproduced with $J_b = -0.0061$, $J_{ab} = -0.030$, and $D_b = -0.37$ meV.

### B. Inchain interactions

The analysis given above rests on the assumption of *flat homogeneous* $CuO_2$ chains, practically unaffected by the incommensurate structure of the adjacent cationic CaY chains, as described in Sec. II. The opposite is depicted in Fig. 1(c) for the simplest case when a symmetric quasiperiod-5 SS is induced in the cuprate chain. A period 10 or 15 would give an even better approximation for the incommensurate SS induced by the strong Coulomb interaction between the differently charged cations and especially the closer O ions of the $CuO_2$

chains. The latter case might be close to an inhomogeneous "lock-in" structure containing "domains" of period 5 and period 10 units as well. Then the two mechanisms of gap production proposed here would be cooperative, resulting in a maximum experimentally observable effect. Since in a general period-$m$ case the opening of $m-1$ gaps is allowed, in the present case one is left with four gaps for a period-5 model while already nine gaps for improved approximations of a period-10 (or even 14 gaps for a period 15) are allowed. The simplest lock-in structure "5 + 10" has 13 gaps. The replacement of the incommensurate SS by a quasicommensurate one containing an *even* period component is essential because it allows the opening of a gap just at the wave vector of 1/4 where the gap near 28 meV has been found. The magnitude of all gaps depends on the distributions of the local Φ and of the distances between NN bridging O ions and also on the twisting and/or other deformations away from the flat structure of ideal chains as in LICO.

Also the dispersion is slightly affected by the opening of gaps if they are included in the fitting procedure (see Sec. V B and Sec. A in the Supplemental Material [7]). Due to the largely increasing number of corresponding couplings probably any distribution of gap amplitudes at the corresponding wave vectors generic for the adopted approximative commensurate SS could be fitted. In this context we do not exclude the possibility of a lock-in transition of the incommensurate cationic chain into a real long periodic commensurate $5m$ periodic chain, where $m = 2, 3, 4,\ldots$. Thus, any real progress by convincing fits should rest on a dialog examination of various local structural models compatible with the diffraction patterns from neutron and x-ray scattering. Improved detailed microstructure models in the real space for inhomogeneous long periodic $CuO_2$ chains have not yet been developed. The examination of such alternative microstructure models with increasing complexity is extremely tedious. Therefore, it is for a future study. Anyhow, we believe that the analysis of the gaps reported here is very important to find effective models with a reasonable number of parameters.

The unexpected lacking of Zhang-Rice excitons in a recent resonant inelastic x-ray scattering (RIXS) study [33], in sharp contrast to LICO and $CuGeO_3$ with "ideal" chains, is noteworthy. We suggest that the expected peaklike feature could not be resolved experimentally due to a relatively broad distribution (more than 0.5 eV) of different "local" excitation energies (at 4.5 eV in LICO) caused by the SS in CYCO. Further consequences of the composite symmetry of CYCO, such as suggested in Refs. [8,34–36] or within the approaches proposed here, will be discussed elsewhere. Figure 3 shows the INS spectra $S(Q, E)$ from our CYCO single crystal measured at 6 K. Figure 3(a) represents the low-energy excitations measured with $E_i = 27$ meV. The intensity is averaged over the range of $1.8 \leqslant K \leqslant 3.2$ and $-0.1 \leqslant L \leqslant 0.1$. The magnon dispersion along $K$ is almost flat and the band width is less than 0.2 meV [21]. Although the band width of the dispersion along $L$ is about 3 meV, the dispersion in the range $-0.1 \leqslant L \leqslant 0.1$ is less than 0.5 meV [21]. Therefore, the broadening due to the integration should be small. On the other hand, the scattering intensity with $E_i = 60$ meV was weak. In order to improve the statistics, the signal was integrated in a wide $Q$ range. In Fig. 3(b) the intensity is

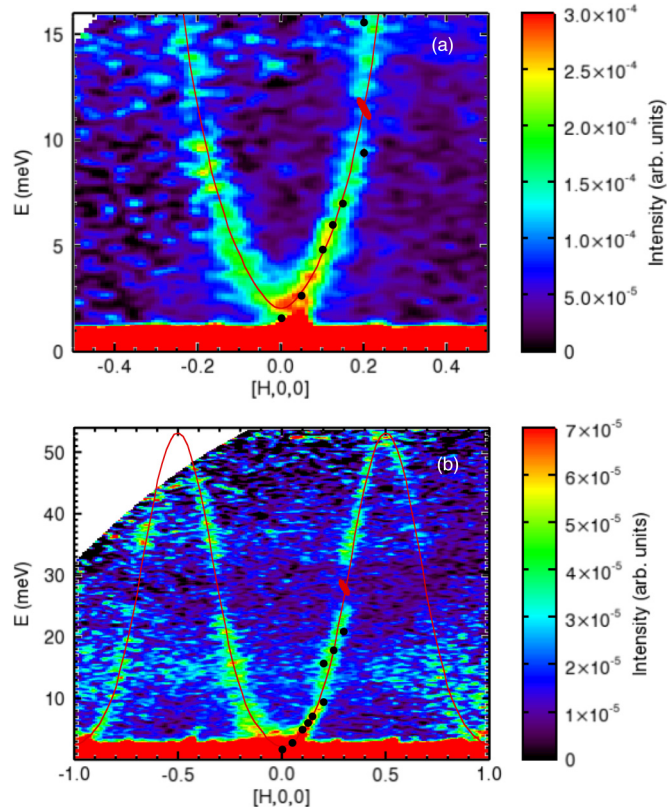


FIG. 3. Contour maps of the INS intensity $S(Q, E)$ for a CYCO single crystal measured at 6 K with $E_i = 27$ meV (a) and 60 meV (b). Energy resolutions at the gap energies are estimated to be ∼0.7 meV at 11.5 meV with 27 meV $E_i$ (a) and ∼2 meV at 28 meV with 60 meV $E_i$ (b). The resolution volumes projected to the $E$-$Q$ space are shown around the gap energies with red ellipses. Filled circles: data points reported in Refs. [21,22]. Solid curves: the dispersion relation calculated using LSWT with $J_1 = -24$, $J_2 = 5.5$, $J_{ac1} = 0.12$, $J_{ac2} = 2.26$, and $D = -0.21$ meV.

averaged over $-0.2 \leqslant L \leqslant 0.2$, where the dispersion width is less than 1.5 meV, and entire $K$ range measured. The range of $K$ depends on the excitation energy, e.g., $0.5 \leqslant K \leqslant 5.5$ at 5 meV and $3.0 \leqslant K \leqslant 4.7$ at 51 meV. Therefore, the effective magnetic form factor gradually decreases with increasing energy and $H$ value, which reduces the averaged intensity. However, the overall dispersion curve can be generated with reasonably good statistics by this method. Figure 3(b) clearly shows a single branch mode along $H$. The characteristic feature is that there are gaplike features at ∼11.5 meV and ∼28 meV, as shown in Figs. 3(a) and 3(b), respectively. The observed magnon dispersion has been analyzed with the help of LSWT (at $T = 0$). For this purpose we have used Eq. (5). We fixed the ICs determined in Sec. III A ($J_{ac1} = 0.12$, $J_{ac2} = 2.26$, and $D = -0.21$ meV). The small $J_c$ was fixed at 0 meV [21] for simplicity, since the dispersion shown in Ref. [21] yields tiny values of −0.061 and 0.037 meV for the NN and NNN couplings, respectively. $J_{a1}$ and $J_{a2}$ were determined from the dispersion along $H$. $J_{a1}$ affects the magnon band width and $J_{a2}$ the dispersion shape in the low-energy region. We found that $J_{a1} = -24$ and $J_{a2} = 5.5$ meV reproduce the overall dispersion, as shown in Figs. 3(a) and 3(b). The

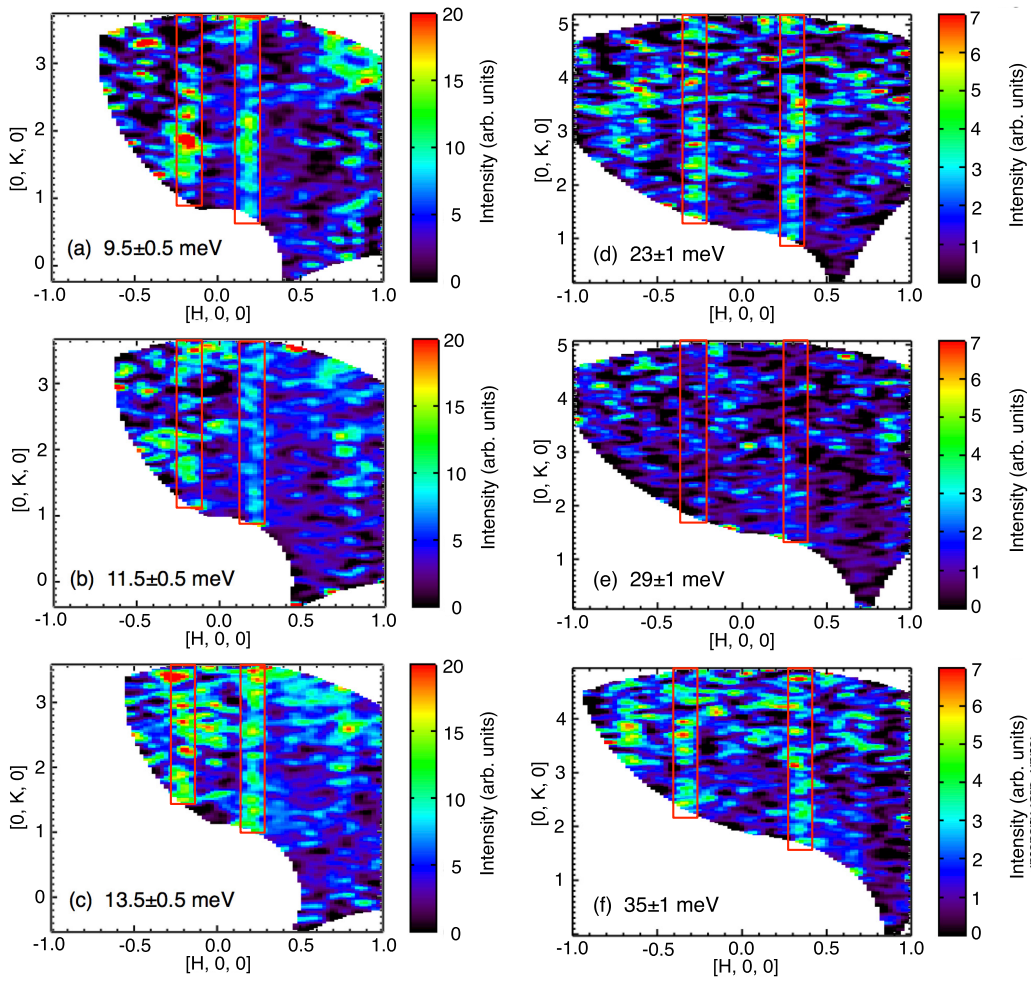


FIG. 4. Energy cuts of the INS intensity in the $(HK0)$ plane measured at 6 K. Spectra at 9.5 (a), 11.5 (b), and 13.5 meV (c), measured with $E_i = 27$ meV and integrated in the range of $-0.1 \leqslant L \leqslant 0.1$. Spectra at 23 (d), 29 (e), and 35 meV (f), measured with $E_i = 60$ meV and integrated in the range of $-0.2 \leqslant L \leqslant 0.2$. Red rectangles: the expected regions for line-shaped magnetic excitations along $K$.

resulting $\alpha = 0.23$ is close to the critical $\alpha_c = 1/4$ (see also Sec. E in the Supplemental Material [7] for the noncriticality of coupled chains).

Noteworthy, the increase by a factor of 3 of $|J_{a1}|$ found over the years (see Table I). Thereby the NNN inchain exchange $J_{a2} \equiv J_2$ has been strongly raised too, while $\alpha$ shows a more moderate increase. Possible disorder effects on the enhancement of $J_2$ in CYCO, $Li_2ZrCuO_4$, and $LiCu_2O_2$ are shown in Sec. I of the Supplemental Material [7]. The unusually small $\alpha$ values in Table I reflect the previous nonoptimal fitting due to the large number of involved couplings. This at first glance surprising result is now well understood. The increase of $|J_1| \equiv |J_{1a}|$ by ~100 K as compared to that from a still nonoptimal fit [24] is very instructive. Good fits can be achieved only by probing the full dispersion, i.e., up to energies $E \geqslant 2|J_1|$, if the third neighbor couplings $(J_3 \equiv J_{3a})$ are reasonably small [9].

### C. Gaplike features

Figure 4 shows six energy cuts in the $(HK0)$ plane through $S(Q, E)$, measured with $E_i = 27$ meV [Figs. 4(a)–4(c)] and $E_i = 60$ meV [Figs. 4(d)–4(f)]. Since the dispersion is almost flat along $K$, there are line-shaped dispersions along $K$, as indicated by red rectangles. Around the gap energies 11.5 and 29 meV, the intensity becomes weak throughout the whole $K$ range, indicating that the structure factor is modified considerably at these specific energies. In particular, the signal is very weak at 29 meV.

To show the intensity more quantitatively, the scattering intensity was plotted as a function of the excitation energy, as shown in Fig. 5(a). The intensity was obtained by fitting the constant energy cut profile with a Gaussian function. In this plot, the integration ranges are $-0.1 \leqslant L \leqslant 0.1$ and $1.5 \leqslant K \leqslant 2.5$ for 27 meV $E_i$ data and $-0.2 \leqslant L \leqslant 0.2$ and $2.5 \leqslant K \leqslant 3.5$ for 60 meV $E_i$ data. The intensities from the two sets of data are normalized using the data points around 20 meV. The correction of the inverse spin-wave velocity was made to convert from the $Q$ integrated intensity to the energy integrated $S(Q, E)$, plotted in Fig. 5(a). The gaplike behavior is distinct at 11.5 and 28 meV. The dip is broader at 28 meV than at 11.5 meV, probably because of the combined effect of broader energy resolution (~2 meV) and wider integration range along $L$, with dispersion width of ~1.5 meV for the 60 meV $E_i$ data. The broader energy resolution with 60 meV $E_i$ also makes the gap at 11.5 meV smeared out [Fig. 3(b)],

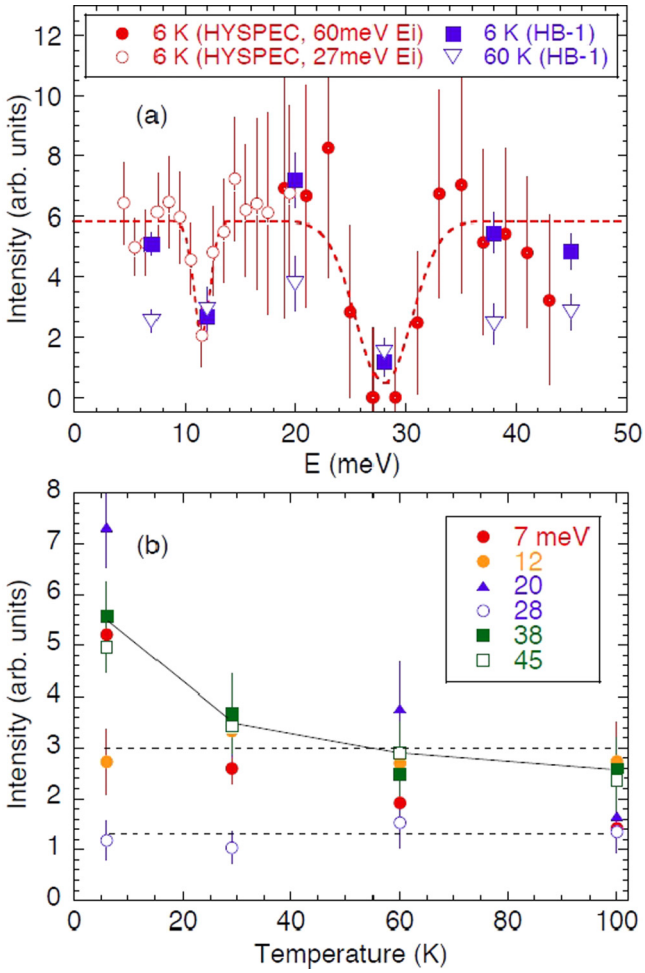


FIG. 5. Energy (a) and $T$ (b) dependences of the integrated intensities from constant energy cuts and scans. Solid and broken lines: guides to the eye. The thick horizontal bars near 11.5 and 28 meV in panel (a) are estimated instrumental resolution.

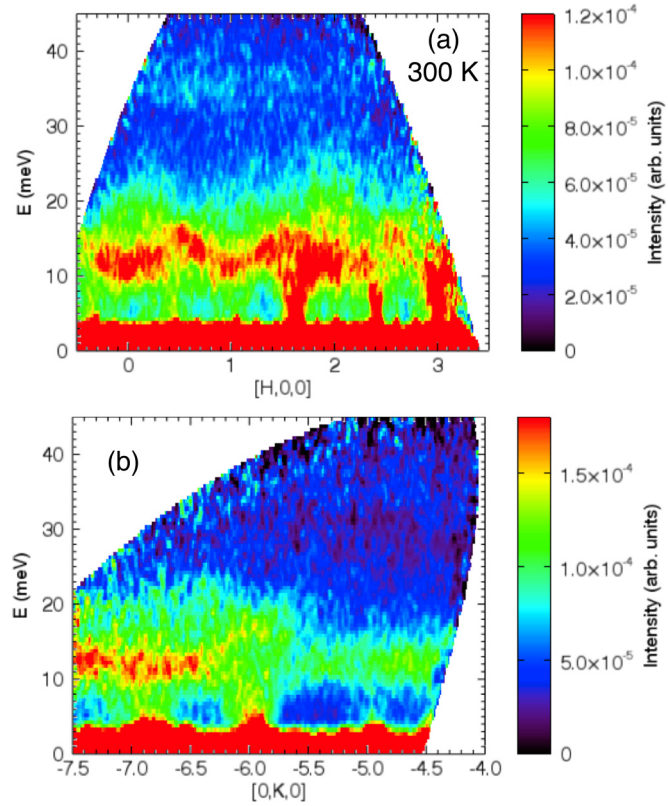


FIG. 6. Contour maps of the phonon dispersions along $H$ (a) and $K$ directions (b) measured at 300 K with $E_i = 60$ meV. The intensities plotted in panels (a) and (b) are integrated in the range of $-6.5 \leqslant K \leqslant -4.5$ and $-0.5 \leqslant H \leqslant 0.5$, respectively.

where the energy resolution is ∼2.5 meV. Except the two dips, the intensity is almost constant throughout the whole energy range, which is expected for ferromagnets. One possibility to explain the gap behavior is the phonon-magnon coupling. Magnons can be interfered when a phonon mode is mixed. A magnon gap due to such an effect was actually reported in $UO_2$ [37–39], $FeF_2$ [40,41], and $La_{1-x}Ca_xMnO_3$ [42]. A gap behavior in the magnon dispersion was also reported for magnetite $Fe_3O_4$ below the Verwey transition temperature ($T$), where charge ordering is expected [43]. The acoustic magnon mode shows a gap at 43 meV and $q = (0, 0, 1/2)$. The origin of the gap is still unknown, although both a charge-density wave and magnetoelastic coupling are considered as possible causes. We examined the phonon dispersions of CYCO carefully. A weakly modulating optical phonon mode along both $H$ and $K$ directions is observed around 11.5 meV, as shown in Fig. 6. This phonon can interfere with the magnon around 11.5 meV. If there exists strong magnon-phonon coupling, a bending of the dispersion curve is usually observed as well as an excitation gap [39]. No such bending was observed in the present measurements. As mentioned in Sec. III, the magnetic signal from the small magnetic moment ($S = 1/2$) in CYCO is weak so that we need to integrate the signal in a wide range of $Q$ region to clearly show the dispersion curve. This integration is likely to make the bending unclear since the optical phonon mode around 12 meV is slightly dispersive. In stark contrast, near 28 meV there is no phonon mode which would intersect the magnon dispersion (Fig. 6). Hence, the latter gap cannot be ascribed to phonon-magnon coupling. As shown above, the $CuO_2$ chains are distorted due to the misfit with the Ca-Y layer. Since the O distortions suggested in Ref. [8] are not so small, some changes of the dynamical structure factor and of the spin-wave dispersion might occur. Our LSWT calculations suggest nevertheless a weak change in the dispersion starting from a homogeneous chain but more pronounced changes in the intensity leading even to the opening of quasigaps have been found (see also Sec. A in the Supplemental Material [7] and below). Much more systematic studies of inhomogeneous models including also Dzyaloshinskii-Moriya (DM) couplings [allowed in that case] and experimental refinement of the structural model are desired to settle quantitatively this very complex problem. Similar studies for CYCO might be of interest too. As first insights we show in Sec. V B and in Sec. A of the Supplemental Material [7] the effect of various simple inhomogeneities. Since $J_{a1}$ amounts to −24 meV (278 K), which is much larger than $T_N = 29.5$ K, a steep magnon dispersion is still expected above $T_N$ along the chain. It is also expected that the dominant IC $J_{ac2}$ (=2.26 meV)

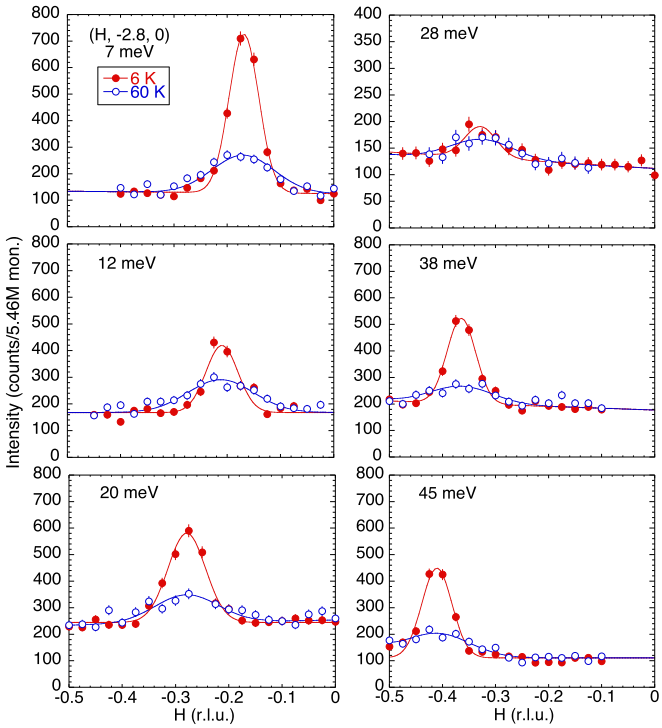


FIG. 7. Constant energy scans at $(H, -2.8, 0)$ measured at $E =$ 7, 12, 20, 28, 38, and 45 meV at $T = 6$ and 60 K. Solid lines are the results of fits with a Gaussian function. r.l.u. represents reciprocal lattice units. To emphasize the peak structure, the vertical scale of the 28 meV data is different from the others.

becomes less effective above $T_N$. Therefore, the effect of the ICs can be elucidated by checking whether the gaplike behavior persists above $T_N$. Figure 7 displays constant-$E$ spectra at 7, 12, 20, 28, 38, and 45 meV, measured at 6 and 60 K on HB-1. The magnetic excitations persist even at 60 K, although the peak width becomes broader. The change of intensity depends on energy. The $T$ dependence of the integrated intensities is shown in Fig. 5(b). Clearly, the intensities at 12 and 28 meV are $T$-independent. On the other hand, those at other energies decrease with increasing $T$. The integrated intensities at 6 and 60 K are shown as a function of energy in Fig. 5(b). The intensities at 6 K are consistent with those measured on HYSPEC. Since the intensities at 12 and 28 meV are unchanged and those at other energies are reduced, the gaplike behavior becomes less distinct at 60 K. Hence, the gaplike behavior at 28 meV is affected by the AFM ICs and is in fact a quantum effect specific for FM chains, as suggested above. The gaplike behavior at 11.5 meV may be due to magnon-phonon mixing, as mentioned above. Then, the magnon-phonon coupling strength might be also weakened at $T > T_N$.

In view of the recently found strong renormalization of the charge transfer energy $\Delta_{pd}$ in the RIXS spectra of LICO by high-frequency O derived modes at 74 meV [44] and near 70 meV for $Ca_{2+5x}Y_{2-5x}Cu_5O_{10}$ with $x = 0$, 0.3, and 0.33 [45] [the latter two being hole ($h$)-doped derivatives of CYCO], the present observation for another active phonon at much lower energy is interesting and deserves to be analyzed also in the general context of electron-phonon coupling in strongly correlated systems. Here INS brings a new low-energy scale not resolved in RIXS studies. Since there is no low-energy gap near 11 meV seen in the INS data of Ref. [9] for LICO, we suggest that it might be an optical phonon derived from the diatomic Ca/Y chain. Then a down shift of that phonon induced gaplike feature might be expected for the sister compound $Ca_2Nd_2Cu_5O_{10}$, having a slightly reduced $T_N = 24$ K [46], and even better with nonmagnetic isovalent substitutions of Y with Lu or Sc. The insertion of magnetic rare earth ions provides additional insight into the cuprate magnetism due to the interplay with the high-spin rare earth subsystem and the check of intrinsic quantum effects. Substitution with Pr might also modify the magnetic structure of the chains through a decrease of the O hole numbers $n_p$ due to the competing covalency with Pr $4f$ electrons, as it happens in $PrBa_2Cu_3O_{7-\delta}$[47], with dramatic consequences for the corresponding $pd$ exchange integrals [Eqs. (5) and (6) in Ref. [47]]. In particular, a strong decrease of $J_1$ might occur, if sizable O $2p$-Pr $4f$ covalency is present. An ordering of the rare earth magnetic moments well above few K (typical for dipole-dipole couplings) in the Pr-based quasi-2D cuprates might explain details of the magnetic response in $Ca_2Nd_2Cu_5O_{10}$ [46]. A systematic study of the whole rare earth series would be interesting. To the best of our knowledge, $Ca_2R_2Cu_5O_{10}$ ($R$ = Dy and Gd) have been synthesized but their physical properties were not studied so far.

## V. THEORY

In addressing the main experimental findings, this section consists of three parts. A and B are devoted to two different phenomenological simulations of the detected midgap, while part C deals with microscopic aspects and consequences of the observed large magnon dispersion.

### A. The midgaplike feature as a quantum effect from diagonal AFM interchain coupling

To understand the gaplike behavior around 28 meV for flat chains, we have first calculated the dynamical spin structure which corresponds to the experimental INS affected also by the form factor. The former is defined as

$$S(q, E) = \sum_{\nu} |\langle \psi_\nu | S_q^{\pm} | \psi_0 \rangle|^2 \delta(E - E_\nu + E_0), \qquad (7)$$

where $S_q^{\pm}$ is the Fourier transform of the spin-flip operator $S_i^{\pm}$ at site $i$ while $|\psi_\nu\rangle$ and $E_\nu$ are the $\nu$-th eigenstate and eigenenergy of the system, respectively ($\nu = 0$ corresponds to the ground state). Two-chain clusters ($32 \times 2$ sites) were studied by using the Dynamical Density Matrix Renormalization Group (DDMRG) method [48]. Open boundary conditions were applied along the chain direction whereas periodic boundary conditions were applied perpendicularly to the chain axis. Then, for an effective two-chain model, ISs are taken to be $2J_{ac1}$ and $2J_{ac2}$ instead of $J_{ac1}$ and $J_{ac2}$. The obtained spectra for some sets of ICs are shown in Fig. 8. The overall dispersion is well described by LSWT with Eqs. (2)–(6) and $J_{ac1} + J_{ac2} \approx 2.29$ meV [24]. Especially for $J_{ac1} =$ 2.29 meV, $J_{ac2} = 0$, a gaplike behavior around $E = 30$ meV is clearly seen. This gap position is close to the INS value of

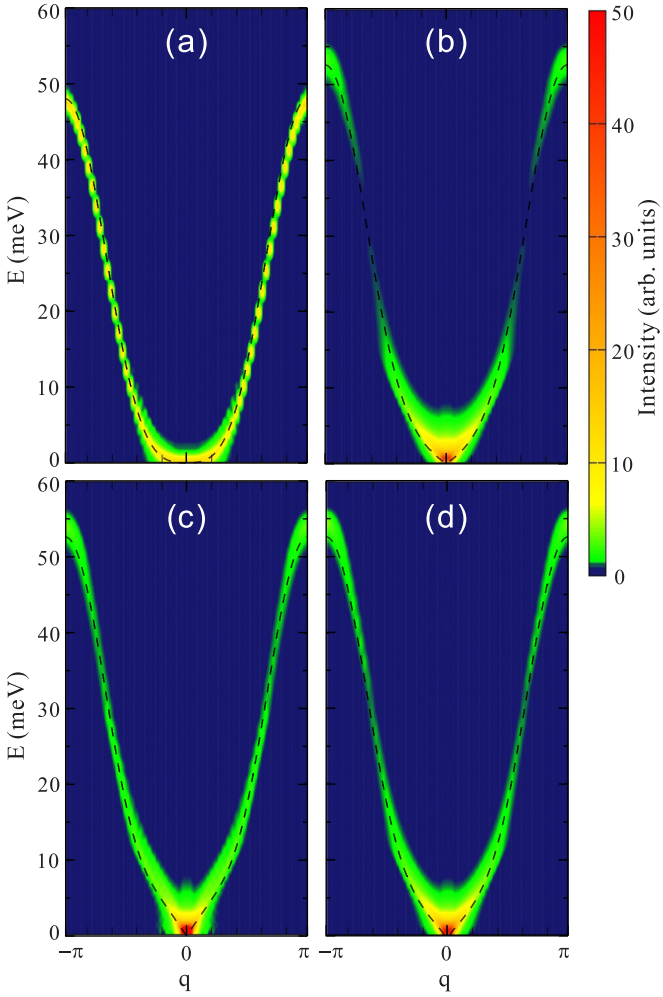


FIG. 8. DDMRG results of the dynamical structure factor $S(q, E)$ with $J_1 = -24$, $J_2 = 5.5$ meV for (a) $J_{ac1} = J_{ac2} = 0$ meV, (b) $J_{ac1} = 2.29$, $J_{ac2} = 0$ meV, (c) $J_{ac1} = 0$, $J_{ac2} = 2.29$ meV, and (d) $J_{ac1} = 1.537$, $J_{ac2} = 0.763$ meV. The dotted lines denote the magnon dispersions $\omega_q$.

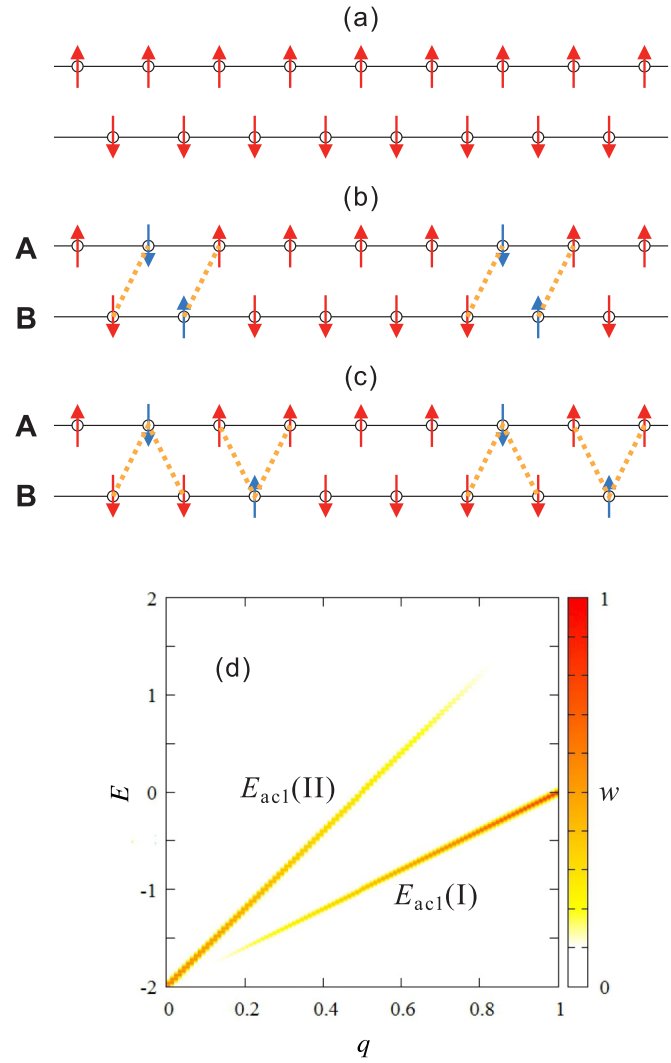


FIG. 9. Schematic spin configurations of (a) the ground state and (b)(c) excited states with $q = 2\pi/5$. Parallel spins are connected by dotted lines and the numbers of the parallel spin pairs are different between panels (b) and (c). (d) Energy contributions by IC $J_{ac1}$ and their weights in the excited states. $q$ is in a unit of $\pi$.

28 meV. The gaplike feature near 28 meV can be understood as a splitting of the excitation levels at an intermediate momentum $q \sim \pi/2$, induced by finite ICs. Let us qualitatively illustrate this by considering the spin configurations at $q = 2\pi/5$. For simplicity, we take two chains coupled by $J_{ac1}$ and employ an Ising-like picture. A representative snapshot of the ground state $|\psi_0\rangle$ is schematically described in Fig. 9(a), where the spins are ferromagnetically aligned along the chain and antiferromagnetically between adjacent chains within the $ac$ plane. Roughly speaking, the operators $S^{\pm}_{q=2\pi/5}$ flip spins on every fifth site on each chain. Thus, spin configurations like **A** and **B** in Figs. 9(b) and 9(c) are created in the excited states $|\psi_\nu\rangle$ when $S^{\pm}_q$ is applied to the ground state $|\psi_0\rangle$. Note that the energies differ between Figs. 9(b) and 9(c). The energy difference comes from interchain contributions which depend on the relative positions of the flipped spins. On the other hand, the intrachain contributions are the same. For Figs. 9(b) and 9(c) the interchain contributions per site are $E_{ac1}(\mathrm{I}) = -\frac{2}{3}J_{ac1}$ and $E_{ac1}(\mathrm{II}) = -\frac{1}{3}J_{ac1}$, respectively. This gives a splitting of the excited energy levels $E_\nu$ in Eq. (7). The ratio of the probability weights is 2:1 since it is proportional to the number of possible combinations of ICs. For arbitrary $q$ we obtain $E_{ac1}(\mathrm{I}) = (\frac{q}{\pi} - 1)J_{ac1}$ and $E_{ac1}(\mathrm{II}) = (\frac{2q}{\pi} - 1)J_{ac1}$, weighted by $w(\mathrm{I}) = \frac{q}{\pi}$ and $w(\mathrm{II}) = 1 - \frac{q}{\pi}$, respectively. In Fig. 9(d) we plot $E_{ac1}$ and $w$ versus $q$. The splitting is zero at $q = 0$ and increases with increasing $q$. Although the splitting is largest near $q = \pi$, it would be less represented in the spectral functions due to the polarized weights, i.e., $w(\mathrm{I}) \gg w(\mathrm{II})$. As a result, such a splitting is most visible around intermediate $q$. To confirm this, we plot the dynamical correlation functions $S(q, E)$ at $q = 0.15\pi$, $0.67\pi$, and $0.97\pi$ for several sets of the ICs in Fig. 10. Without ICs ($J_{ac1} = J_{ac2} = 0$) *no* splitting is seen for any $q$ [Fig. 8(a)]. But for finite ICs, the splitting is clearly confirmed at the intermediate momentum $q = 0.67\pi$ [Fig. 10(b)]. This feature is most obvious for $J_{ac1} = 2.29$ meV and $J_{ac2} = 0$ [Fig. 8(b)].

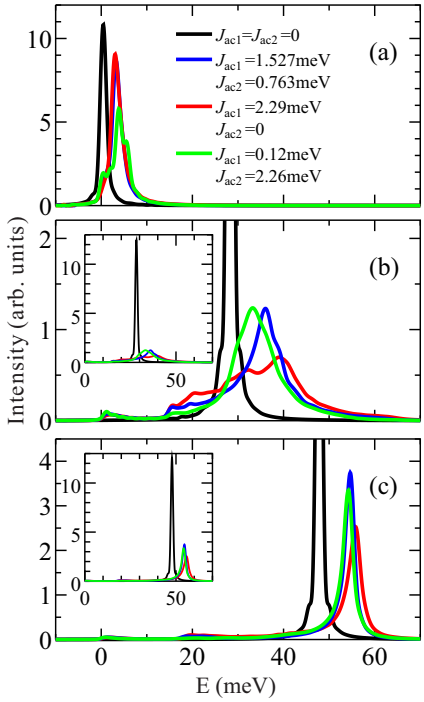


FIG. 10. DDMRG results of the dynamical correlation functions $S(q, E)$ at (a) $q = 0.15\pi$, (b) $0.67\pi$, and (c) $0.97\pi$. Insets display the entire range of the intensity.

The splitting causes a continuum by quantum fluctuations, and it appears as a broadening of the intensity in the spectrum. At lower ($q \approx 0$) and higher ($q \approx \pi$) momenta, the peak height is reduced by the ICs, but they are still sharp, only with a slight broadening [Figs. 10(a) and 10(c)]. The significant broadening at the intermediate momenta ($q \approx \pi/2$) provides a lack of $q$ integrated intensities at intermediate energies $E$, which corresponds to the experimental dip of the $Q$ integrated intensity. The broadening is less pronounced for other ICs, pointing to a gaplike behavior most pronounced for a larger $J_{ac1}/J_{ac2}$ ratio. In fact, the gaplike feature is less obvious for $J_{ac2} > J_{ac1}$ [Figs. 8(c) and 8(d)].

### B. Gaps from inhomogeneous $CuO_2$ chains

Here we briefly illustrate where gaps in the magnon curve can appear within the adopted period-10 scenario for the cationic Ca/Y chain system, ignoring thereby ICs for simplicity. Let us assume that the lattice modulation leads to small deviations from the ion positions in the flat homogeneous chain, i.e., $R + s \approx na$ "in average." We consider a single chain where the structural modulations cause an alternation of the exchange couplings. The spin-Hamiltonian of a chain with a basis reads

$$\hat{H}_{ch} = \frac{1}{2}\sum_{R,s,r_s}\left[J_{r_s}\hat{\mathbf{S}}_{R+s}\hat{\mathbf{S}}_{R+s+r_s} + D_{r_s}\hat{S}^z_{R+s}\hat{S}^z_{R+s+r_s}\right], \tag{8}$$

$$\approx \sum_{R,s}\left[\varepsilon_{R+s}a^\dagger_{R+s}a_{R+s} + \frac{1}{2}\sum_{r_s}J_{r_s}a^\dagger_{R+s}a_{R+s+r_s}\right], \tag{9}$$

$$\varepsilon_s \equiv \frac{1}{2}\sum_{r_s}\left(J_{r_s} + D_{r_s}\right). \tag{10}$$

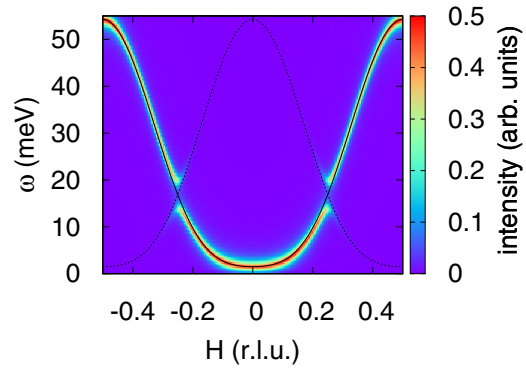


FIG. 11. The dynamic structure factor $S(q, \omega)$ for the $J_1$-$J_1'$-$J_2$ model. $J = -26.38$, $J_2 = 5.5$, $\delta = 3$, and $D = -1.5$ meV. Thin line: the twofold supercell with $\delta = 0$ (see analogous features in Fig. S1 of the Supplemental Material [7] for the case of a fivefold supercell).

where $R$ counts the cells and $s$ the sites within the cell, $r_s$ defines the neighbors coupled with the site $s$; in Eq. (9) we expressed the spin-Hamiltonian in terms of spin deviation operators using the Holstein-Primakoff bosonization assuming a FM ground state of the chain.

We have calculated the structure factor in the large Brillouin zone $-\pi/a < q \equiv 2\pi h < \pi/a$:

$$S(q,\omega) \propto -\mathrm{Im}\left(\left\langle\left\langle \hat{S}^x_q|\hat{S}^x_{-q}\right\rangle\right\rangle_\omega + \left\langle\left\langle \hat{S}^y_q|\hat{S}^y_{-q}\right\rangle\right\rangle_\omega\right)$$
$$\approx -\tfrac{1}{2}\mathrm{Im}(\langle\langle a_q|a^\dagger_q\rangle\rangle_\omega + \langle\langle a_q|a^\dagger_q\rangle\rangle_{-\omega}), \tag{11}$$

where

$$a_q = \frac{1}{\sqrt{Nn}}\sum_{R,s}\mathrm{e}^{-iq(R+s)}a_{R+s} \equiv \frac{1}{\sqrt{n}}\sum_s \mathrm{e}^{-iqs}a_{q,s},$$

where $N$ is the number of cells, $n$ is that of sites per cell.

In Fig. 11 we show how a twofold SS of the $J_1$ values (compatible with a period-10 SS) affects the intensity of the calculated LSWT dynamical spin structure factor $S(q, \omega)$. Notice the absence of shadow bands and the slightly changed dispersion visible in the height of the maxima (lowered here by ∼5 meV) probably due to the omitted ICs. In order to "fit" the observed dispersion and the main gap near 28 meV, the remaining couplings have to be changed too. Thus, the SS does not only open gaps as expected, but it also changes the dispersion also far from the gap [49].

### C. Theoretical aspects of large FM $J_1$ values

Despite some exceptions, including $CuGeO_3$ (all due to large $\Phi$ and the presence of strong crystal fields), $J_1$ is usually FM (see Table I in the Supplemental Material [7]). $J_1 = -24$ meV in CYCO is remarkable. It exceeds $J_1$ of LICO ($-19.6 \pm 0.4$ meV) and also that of $Li_2ZrCuO_4$ slightly ($-23.5$ meV) [4]. Since a highly dispersive magnon gives dynamical evidence for a strong FM NN $J_1$, it deserves a phenomenological and microscopical analysis and verification by other data. We start with an analysis of the magnetic susceptibility $\chi(T)$ and then continue with microscopic aspects of the closely related LICO with a simpler but similar averaged structure as CYCO. The validity of the large $J_1$

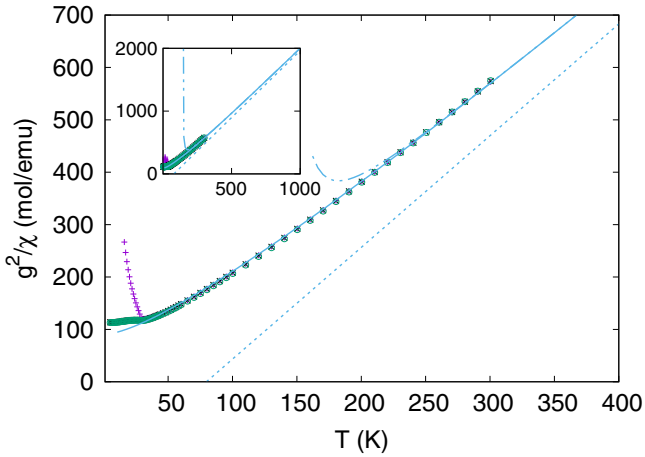


FIG. 12. The inverse spin susceptibility for a magnetic field along the $a$ (×), $b$ (+), and $c$ (○) axes of CYCO (from Ref. [50]). Dashed double-dotted line: fit by the 10th-order HTE Eq. (13); solid line: [5,5] Padé approximation. Short-dashed line: the exact CW asymptotic curve. Inset: Extended $T$ range up to 1000 K.

regime is also confirmed by several DFT + $U$ calculations for LICO [9].

#### 1. Consequences for the magnetic susceptibility

Ignoring the tiny FM couplings along the $b$ axis, CYCO is a 2D Néel system with a relatively large FM Curie-Weiss (CW) temperature:

$$\Theta_{\rm CW} \approx -\tfrac{1}{2}[J_{a1}(1-\alpha) + z(J_{ac,1} + J_{ac,2})] \approx 80\ {\rm K}, \qquad (12)$$

where $2z$ measures the number of NN and NNN sites on the adjacent chains. Without the ICs one would arrive at $\Theta_{\rm CW} \approx$ 107 K. To show that the exchange values determined from our refined INS measurements are fully compatible with the $\chi(T)$ data, we reproduce in Fig. 12 the data from Ref. [50]. Similarly to our recent analysis of $\chi(T)$ for LICO [11], we have fitted the data in the range $240 < T < 300$ K with the expression

$$\chi(T) = \frac{5N_A g^2 \mu_B^2}{k_B}\chi_{10}(T), \quad \chi_{10}(T) = \sum_{n=1}^{10}\frac{c_n}{T^n}, \qquad (13)$$

where $\chi_{10}(T)$ is the 10th-order HTE [51,52]. $N_A$ is the Avogadro number (one mole of CYCO contains $5N_A$ spins), $\mu_B$ is the Bohr magneton, and $g$ is the gyromagnetic ratio. A small anisotropy of the couplings as well as the tiny interplane couplings ($J_b/k_B, J_{ab}/k_B < 1$ K) is unimportant for the $\chi(T)$ analysis and was ignored here. Evidently, the HTE series, Eq. (13), fits well the data for $g_a \approx 2.04$, $g_b \approx 2.28$, $g_c \approx 2.02$ above $T \sim 240$ K. We recall that an ESR study on powder samples of CYCO reports $g_b \approx 2.31$ and $g_\perp \approx 2.03$ [53]. The [5,5] Padé approximation fits the curve down to $T \gtrsim T_{\rm N}$. Figure 12 also shows the CW asymptotic curve, reached only at $T \gtrsim 1000$ K, as shown in the inset. From this comparison the strong IC in CYCO is evident, explaining the *absence* of criticality, which manifests itself in a strong upshift of $\alpha_c$ (see the Supplemental Material [7]) and in the large moments seen in neutron diffraction in the quasi-2D Néel state below the high $T_N \approx 30$ K. In contrast, LICO, $Ca_2Nd_2Cu_5O_{10}$, and $CuAs_2O_4$ might be closer to the 1D $\alpha_c$ due to $\alpha > 1/4$ and a much weaker AFM IC, which is even there necessary to stabilize a FM alignment. For LICO the analogous AFM IC $J_{bc,1} + J_{bc,2}$ is only 9 K (0.8 meV) per bond, where the $b$ axis is the chain direction.

To avoid such strange results found often in the literature from improper $\chi(T)$ fits (e.g., $\Theta_{\rm CW} = 2$ K [14] for CYCO), low-$T$ INS (or RIXS) probing the magnon dispersion, combined with magnetization data up to the saturation field, allows to extract more reliable couplings. The former should be used to cross-check any exchange set derived from $\chi(T)$, if multiple $J'$s are involved. Noteworthy, for $La_6Ca_8Cu_{24}O_{41}$ [54] containing both *undoped* TLL and $CuO_2$ chains just like in CYCO but with a *smaller* $\Phi$, a tiny $\Theta_{\rm CW} = 21 \pm 1$ K has been reported [54] from linear fits of $1/\chi(T)$ data up to 300 K only. But from that $\Phi \approx 91.6^\circ$ according to Eqs. (14), (16), and (18), even a *larger* FM $J_1$ is expected. Then, with a smaller AFM IC due to the low $T_{\rm N} \approx 12.5$ K and a similar misfit from $La^{3+}$ replacing $Y^{3+}$, as in CYCO, a much *larger* $\Theta_{\rm CW} \sim 100 \gg 21$ K is requested. Another related issue is the incorrectly predicted critical $h$-doping when $\Theta_{\rm CW}$ changes its sign, i.e., for weak $h$-doping a sizable magnon dispersion and hence $\Theta_{\rm CW} > 0$ are still expected, at odds with the opposite sign provided so far in the literature from improperly fitted asymptotics. Our dispersion-law (with a generalization for frustration perpendicular to the AFM 2nd adjacent chain [55] as proposed for $La_5Ca_9Cu_{24}O_{41}$) allows to separate chains from ladders dominant above their spin gap [56].

Since frustrated FM systems are of general interest in the field of quantum magnetism and statistical physics [57–59], hopefully, our work will initiate further work. In particular, systematic studies of critical systems like $CuAs_2O_4$ with $\alpha \approx 0.27$ [60–62] will give insight into the role of quantum fluctuations (see Table I in the Supplemental Material [7]). In this context the study of other thermodynamic properties as the specific heat and thermal conductivity might be useful to check the coupling constants derived here. Other examples of weakly $h$-doped compounds [34,63] will be addressed elsewhere.

#### 2. QC and DFT analysis for LICO—Comparison with Mizuno et al. [15]

The most notable theoretical finding of the present work with respect to an empirically large FM $J_1$ value is several microscopic FM intersite couplings behind the spin-chain model, obtained by QC and DFT-based analysis. Given the complex real structure of CYCO, we will present theoretical studies for LICO since its structure is very close to the *averaged idealized* structure of CYCO. In fact, their Cu-O-Cu bond angles $\Phi$ differ by $\approx 0.1^\circ$, whereas the Cu-Cu distances $d_{\rm Cu-Cu}$ by 0.04 Å and the Cu-O bond length $d_{\rm Cu-O}$ by $\approx$0.025 Å only [35,64]. We therefore believe that the NN results for LICO can be transferred to CYCO with an uncertainty of only a few percents. A semiquantitative general analysis including several cuprates will be given elsewhere. Providing refined theoretical results for LICO very much simplifies the modeling and allows a critical check of the parameters *adopted* in Ref. [15] for LICO. It is convenient to decompose

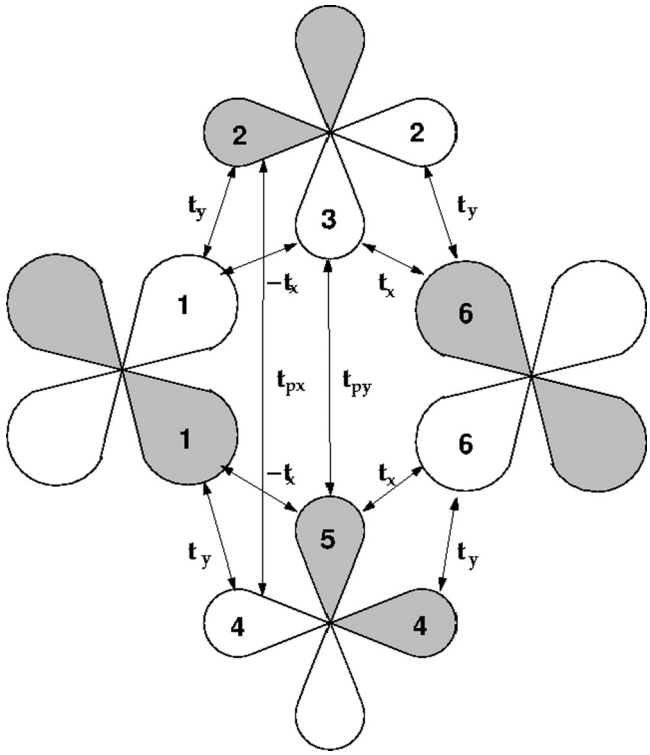


FIG. 13. $p$ and $d$ orbitals and transfer integrals of a $CuO_2$-cluster treated exactly within a planar Cu $3d$ O $2p$ five-band Hubbard model: Cu $3d_{xy}$ 1 (left) and 6 (right); intermediate O $2p_{x,y}$ 2,3 (upper) 4,5 (lower). The chain is along the horizontal direction ($x$ axis). For the sake of clarity the hopping $t_{dd}$ between two Cu sites along the $x$ axis is not shown.

the total $J_1$ into a FM and an AFM contribution:

$$J_1 = J_1^{\rm FM} + J_1^{\rm AFM}, \quad \text{with} \tag{14}$$

$$J_1^{\rm FM} \approx J_1(K_{pd}, K_{pp}) + J_1(J_H) - K_{dd} \quad \text{and} \tag{15}$$

$$J_1^{\rm AFM} \approx J_\Phi + \frac{4t_{dd}^2}{U_d - V_{dd}}, \tag{16}$$

where $K_{pd}$, $K_{pp}$, and $K_{dd}$ denote direct FM *intersite* Coulombic (Heisenberg) exchange integrals and $J_H$ is the indirect *onsite* Hund's rule coupling from each of the bridging O's. For the corresponding $pd$-Hamiltonian, see, e.g., Refs. [15,44,65,66] and Fig. 13. The generalization including also the Cu-Cu intersite terms $K_{dd}$, $V_{dd}$, and the hopping $t_{dd}$ (all ignored there) is straightforward. For enlarged $K_{pd}$ and $K_{pp}$ in the 2D geometry of $La_2CuO_4$, see Refs. [16,17].

Turning to the various FM sources in $J_1^{\rm FM}$ entering Eq. (15), we note that in general all fundamental FM exchange couplings are known by order of magnitude only: 1 meV $<$ $K_{dd} \ll K_{pp} \ll K_{pd} \ll J_H <$ 1.5 eV. To the best of our knowledge, the direct intersite exchange interactions $K_{pd}$, $K_{dd}$, and $K_{pp}$ reported here have not been calculated or estimated so far for chain cuprates. Refining the estimates given above, our QC result is $K_{dd} \approx 4.2$ meV, indeed much smaller than various $K_{pp} < 20$ meV, and $K_{p_xd} \approx K_{p_yd} \approx 105$ meV (for details see Sec. C in the Supplemental Material [7]). $J_H$ somewhat

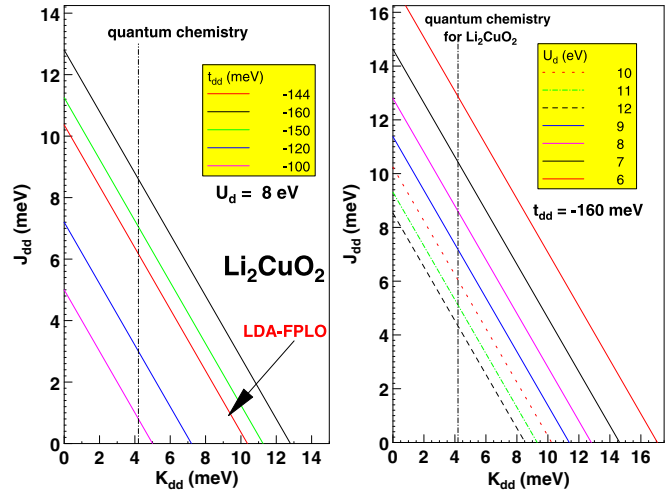


FIG. 14. Superexchange from the $dd$ channel $J_{dd}$ vs the direct intersite FM exchange $K_{dd}$ for various direct Cu-Cu hoppings $|t_{dd}|$, e.g., $t_{dd} = -144$ ($-160$) meV by LDA (QC) mapping (both ignored in Ref. [15]; for details, see Sec. C in the Supplemental Material [7]) (left) and adopted onsite Hubbard $U_d$ values (right). Vertical dashed-dotted lines are the QC result for LICO.

exceeds the value of 600 meV adopted in Ref. [15]. According to direct calculations and various empirical estimates, in particular, for related superoxides [67], a bit enhanced slightly screened $J_H$ value $\sim$0.7 eV is even more realistic [68]. $K_{pd}$ turns out to be the most important FM microscopic interaction for $J_1$ since a weak enhancement of a moderate $J_H$ cannot explain the more than twice as large $J_1$ at fixed $K_{pd} = 50$ meV universally adopted by Mizuno *et al.* [15] (including also CYCO) who found $J_1 = 100$ K for LICO at odds with $|J_1| \geqslant$ 230 K derived without fully probed by INS [9] magnon dispersion leaving therefore some room for further refinements in future if the same sophisticated intensity analysis as in Sec. IV for CYCO could be applied there too.

Our DFT and QC analysis succeeded also in the determination of a remarkable direct $dd$ transfer integral $|t_{dd}|$, 144 and 160 meV, respectively, due to the short NN Cu-Cu distance $d_{\rm Cu-Cu} \approx 2.86$ Å. A finite $t_{dd}$ (ignored in Ref. [15]) provides an *additional* AFM contribution if

$$\left|t_{dd}^c\right| > 0.5\sqrt{(U_d - V_{dd})K_{dd}}. \tag{17}$$

Typically $J_{dd}$ is of the order of $+5$ meV (Fig. 14), yielding further arguments for a larger $K_{pd}$. With this AFM $dd$ channel alone, $J_1 \approx 165$ K would be achieved when fixing $K_{pd}$. The precise value of $U_d$ (actually unknown) affects strongly the efficiency of the $dd$ AFM superexchange, as shown in Fig. 14, especially for FFESC cuprates with a short Cu-Cu distance. It markedly exceeds that for typical charge transfer insulators ($U_d \gg \Delta_{pd}$), where it is negligible due to the tiny $t_{dd}$. Also a realistic intersite Cu-Cu Coulomb interaction $V_{dd}$ of 0.3 to 0.5 eV [69–72] might be relevant [compared to Eqs. (23), (24), and (S24) and Sec. J in the Supplemental Material [7]]. The $dd$ channel is of interest for further theoretical studies since it gives a new Cu-Cu-O-Cu exchange path in addition to the known Cu-O-O-Cu one, with possible modifications of $J_2$.

#### 3. Comparison with other cuprates and general trends

Looking for an empirical support, we will compare our $J_1$ values with those of other cuprates and provide thereby a critical analysis for the exclusive attempt to present a general description of edge-sharing chain cuprates and ladders performed 20 years ago [15], when almost no detailed microscopic studies were known. We will show that it is timely to reconsider not only LICO and CYCO since our criticism concerns the unjustified use of a systematically *underestimated, universal*, and *isotropic* direct FM Cu-O exchange $K_{pd} =$ 50 meV [15] with serious consequences for the FM $J_1$. It is in fact of general interest for all cuprates with edge-sharing elements, including infinite $CuO_2$ chains, ladders, coupled $Cu_nO_{n+2}$ ($n = 2, 3, 4,...$), and other finite edge-sharing $CuO_4$ units (see Table I of the Supplemental Material [7]). This provides the basic picture of the interactions in cuprates and the minimal stage for the five-band Hubbard *pd*-model in terms of which their fundamental physical properties must be discussed.

The magnitude of the NN exchange is important for any quantum magnet, in particular, for cuprates with edge-sharing elements present in single and double (zigzag) chains, since it determines or strongly affects the role of frustration measured here by $\alpha$ in Eq. (1).

As mentioned above, $\alpha \gg 1$ can be treated as an effective AFM system with slightly renormalized $J_2$ values ignoring the finite $\alpha^{-1}$ value at all. Unbiased QC and DFT studies allow insight into the magnitude of $J_1$, despite some uncertainty due to certain correlation and spin-orbital effects ignored here. With this in mind, we select and comment on available data for various cuprates in Table I of the Supplemental Material [7]. Naturally, $\Phi$ near 90°, the Cu-Cu $d_{\mathrm{Cu-Cu}}$ and the Cu-O distances within the generic $CuO_4$ plaquettes as well as the strength of the crystal field, strongly affected by the charge and position of the surrounding cations near the bridging O, are important physical ingredients.

Similar or even larger $J_1$ values have been observed or predicted by theoretical studies [73–75] so far only in (i) ladder compounds ($J_1$ corresponding to the interladder couplings), (ii) double-corner-sharing (zigzag) chain compounds with predicted $J_1$ values of $-28$ to 55 meV, and (iii) alternating FM-AFM chain systems $Li_3Cu_2SbO_6$ [76] and $Na_3Cu_2Sb(Te)O_6$ [73] with $J_1 = -23.56$ meV. $Li_3Cu_2SbO_6$ [76] and $Na_3Cu_2SbO_6$[73,77,78], with similar AFM couplings but very different relatively large FM $J_1$ values, are particularly striking. In view of its large $\Phi = 95.27°$, an AFM or very weak FM coupling would be expected according to Ref. [15]. Hence, an enlarged FM interaction and/or a strongly suppressed AFM exchange via the bridging O must be responsible for the resulting FM $J_1 = -17.8$ meV, twice of $-8.6$ meV estimated for $\Phi = 93.97°$ (the case of LICO) [15]. The smaller value of $-12.7$ meV derived from INS data [78] is probably due to the too small limiting energy of 14.7 meV probed there, similarly as for CYCO previously. There the $CuO_2$ chains are distorted by a similar cationic misfit, as in CYCO, in the combined TLL and chain system $La_6Ca_8Cu_{24}O_{41}$. Due to the $\Phi$ closer to 90° also somewhat larger $J_1$ values are expected. Unfortunately, its chain magnon component is not yet fully understood, hampered by the dominant two-spinon contribution and the *h*-doping in some cases [79]. Our present $J_1$ value strongly exceeds an earlier estimate of $-2.15$ meV for CYCO and that of $-8.6$ meV for LICO [15]. Furthermore, it is at odds with $\alpha = 2.2$ [15] and puts it close to $\alpha_c$. The results from QC analysis for LICO show a markedly enlarged $J_1$ by 42% as compared with Ref. [15] but not enough when compared with the empirical and DFT-derived values with a still larger 130% enhancement. For the TLL $SrCu_2O_3$ a less dramatic but also enhanced value by about 15% was predicted, which, however, is caused by the smaller $\Phi$ (see also Ref. [79]). For $\Phi = 90°$, generalizing an expression for $J_2$ by the account of a moderately enhanced direct FM *pd* intersite *h*-exchange $K_{pd}$, $\alpha \approx 3$ to 4 is estimated, as shown below. Then based on the empirical $J_2 \approx 166$ meV, $J_1 \approx -55$ to $-41.5$ meV can be estimated for $SrCu_2O_3$ as an upper bound and we would arrive at $J_1 \approx -38 \pm 1$ meV as a realistic estimate. Note that again it exceeds the value from Ref. [15], now by ≈25% and $J_1^{\mathrm{FM}} = -38$ meV like in LICO. Thus, one has enough reasons to doubt the results given there for various chains and ladders. Then one may ask: "What is the reason for the *material-dependent* systematic underestimates given in Ref. [15]?" The numerous examples discussed above require a strong material dependence which is unlikely for $J_H$. But its efficiency is lowered for split O onsite energies due to strong crystal field effects. In addition the usual indirect superexchange $J_\Phi$ via the bridging O increases and one can easily arrive at small $J_1$ values ∼80–100 K, as realized, e.g., in linarite with a moderate $\Phi \approx 93°$. Then $K_{pd}$ remains the main microscopic source for FM $J_1$ values in cases as LICO since only a weak material dependence of $J_H$ (governed mainly by $U_p$) is expected. The *two* interacting bridging O ions cause a slower convergency of standard perturbation theory, used previously to the effect of $K_{pd}$ and $J_H$. Hence, exact diagonalizations on small clusters are used to study this point, as shown in Figs. 15 and 16.

#### 4. Description in the five- and single-band Hubbard models

Now we will show semiquantitatively that a realistic microscopic scenario for such large FM $J_1$ values well exceeding $-200$ K can be proposed. Our arguments will be expressed in terms of the most natural and vivid multiband Cu $3d$ O$2p$ Hubbard model with five magnetically active orbitals in the $xy$ plane containing ideally flat $CuO_2$ chains, namely, the single Cu $3d_{xy}$ orbital and the two O $2p_x$ and $2p_y$ orbitals for each of the two bridging O (Fig. 13), where $x$ is the chain axis ($a$ axis in Fig. 1) and the $y$ axis corresponds to the crystallographic $c$ axis (see also the Supplemental Material [7]). Since this model contains already a large set of partly not precisely known interactions, we consider below also an effective single-band model with a reduced number of parameters. The first *pd* term of the AFM contribution according to standard 4th-order perturbation theory [80,81] reads

$$J_\Phi \approx \frac{4t_{p_xd}^2}{\left(\Delta_{p_xd}+V_{p_xd}\right)^2}\left[\frac{2t_{p_xd}^2}{\Delta_{p_xd}+V_{p_xd}}+\frac{1}{U_d}\right] - \frac{4t_{p_yd}^2}{\left(\Delta_{p_yd}+V_{p_yd}\right)^2}\left[\frac{2t_{p_yd}^2}{\Delta_{p_yd}+V_{p_yd}}+\frac{1}{U_d}\right]$$

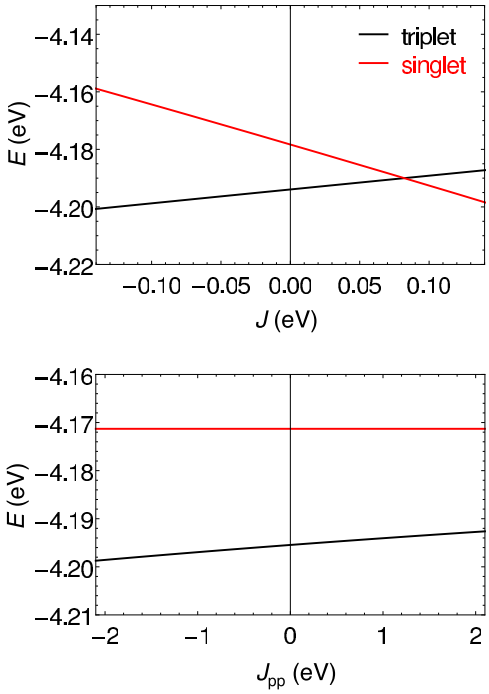


FIG. 15. Lowest singlet and triplet energies of a $\Phi = 90^\circ$ $CuO_2Cu$ cluster as in Fig. 13 vs the main FM exchanges for a set close to Ref. [15], where a $O_2$-$CuO_2Cu$-$O_2$ cluster was used. ($t_{p_xd} = t_{p_yd} = 0.7155$, $t_{dd} = 0$, $t_{p_x} = 0.17$, $t_{p_y} = 0.69$, $V_{pd} = V_{dd} = J_{dd} = 0$, $\Delta_{pd} = 3.2$, $E_{p_x} = 1.75$, $E_{p_y} = 1.45$, $U_d = 8.5$, $U_p = 4.1$, $K_{pd} = 0.05$, and $J_H = 0.6$; all in hole notation and in units of $t \equiv t_{pd} \approx 1$ eV) $J = -K_{pd}$ (upper plot for $J_H = 0.6$) and $J_{pp} = -J_H$ at $K_{pd} = 0.05$ (lower plot).

$$\approx \frac{4t_{pd}^2 \sin^2 \Phi/2}{(\Delta_{p_xd} + V_{pd})^2}\left[\frac{2t_{pd}^2 \sin^2 \Phi/2}{\Delta_{p_xd} + U_p} + \frac{1}{U_d}\right] - \frac{4t_{pd}^2 \cos^2 \Phi/2}{(\Delta_{p_yd} + V_{pd})^2}\left[\frac{2t_{pd}^2 \cos^2 \Phi/2}{\Delta_{p_yd} + U_p} + \frac{1}{U_d}\right] \approx -\frac{4t_{pd}^2}{(\Delta_{pd} + V_{pd})^2}\left[\frac{2t_{pd}^2}{\Delta_{pd} + U_p} + \frac{1}{U_d}\right]\cos\Phi\,, \quad (18)$$

ignoring for shortness the O-O NN hopping terms [compare to Eqs. (S46) and (S47) in the Supplemental Material [7] for the case $\Phi = 180^\circ$, where the last equation is obeyed in the isotropic limit]. It vanishes for $\Phi = 90^\circ$, if one ignores the slightly different O $2p_x$ and $2p_y$ onsite energies due to the weak crystal field [72]. In contrast, in cases of strong crystal fields or the presence of ligands, even at $\Phi = 90^\circ$ there is a significant AFM contribution that reduces the total value of $J_1$. For the experimental value of $\Phi$ and by adopting the parameters of Ref. [15], i.e., ignoring first of all the intersite Coulomb interaction $V_{pd}$, one has $J_\Phi \approx 200$ K. Since $J_1^{\rm AFM}$ depends markedly on $\Phi$, the total $J_1$ may change its sign at $\Phi$ values far enough from $90^\circ$, which happens in fact in several cases different from LICO and CYCO (see Table I in the Supplemental Material [7]).

$K_{pd}$ and $J_H$ occur in reverse orders of the $(t_{pd}/\Delta_{pd})$-perturbation theory affecting their weight and $n_p$ on the two O sites which interact by hoppings and FM $K_{pp}$. In the spirit

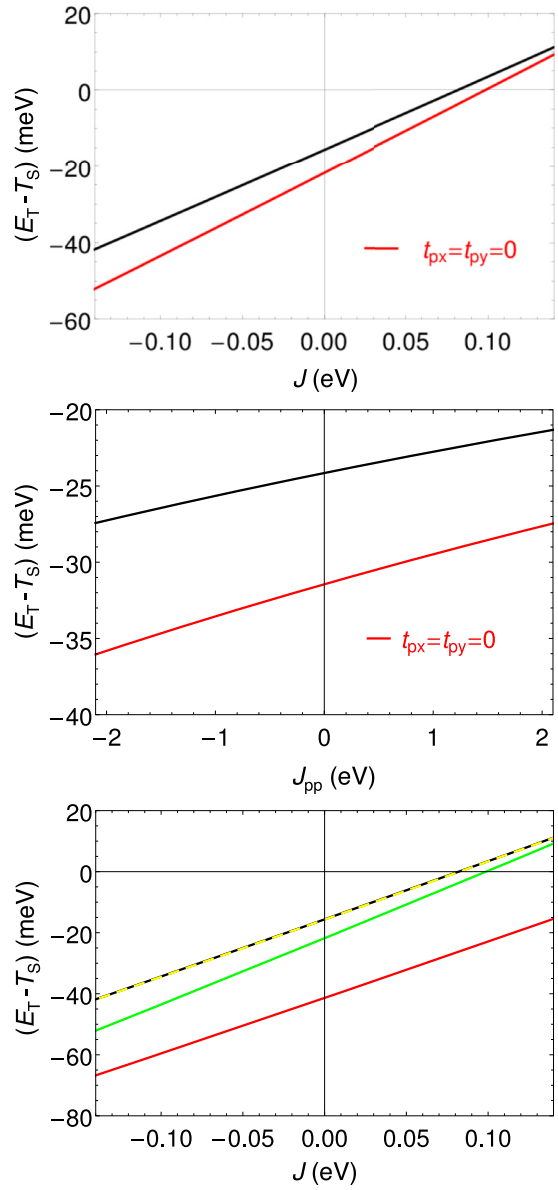


FIG. 16. The NN exchange $J_1 = E_T - E_S$ from exact diagonalizations similarly to Eq. (19). The suppression of the intersite interaction between the "upper" and lower O for $U_p = \infty$ (green curve) and $t_{p_yp_y} = t_{p_xp_x} = 0$ (red curve) as compared to the set described above (black curve). Dotted curve: including also the weak FM direct exchange $K_{pp}$ ($K_{p_yp_y} = 18.4$, $K_{p_xp_y} = 13.4$, and $K_{p_xp_x} = 8.7$ meV).

of this approach for the five-band Hubbard model sketched in Refs. [81,82] for the case of edge-sharing plaquettes with two common O, Eq. (15) can be approximated by

$$J_1^{\rm FM} \approx -K_{dd} - 8Z\left(\frac{t_{pd}}{\Delta_{pd}}\right)^2 K_{pd} - \frac{4Z^2 J_H}{(1 + U_{pp}/\Delta_{pd})}\left(\frac{t_{pd}}{\Delta_{pd}}\right)^4 \approx -K_{dd} - 4\left(\frac{t_{pd}}{\Delta_{pd}}\right)^2 K_{pd} - \frac{J_H}{(1 + U_{pp}/\Delta_{pd})}\left(\frac{t_{pd}}{\Delta_{pd}}\right)^4, \quad (19)$$

where the renormalization factor $Z(t_{pp}^2/U_p, K_{pp}, \Delta_{pd}) < 1$ has been introduced. It contains higher-order corrections due to

various O-O hoppings and direct FM couplings $K_{pp}$ taken from our DFT and QC analysis.

For $\Delta_{pd} = 3.5$ eV, $Z \approx 0.48$. A quasilinear law for $J_1$, $K_{pd}$, and $J_H$, like in Eq. (19) (with slightly changed second and third coefficients due to additional interactions) holds, also beyond $(t_{pd}/\Delta_{pd})$-perturbation theory as confirmed by the exact treatment of Cu-$O_2$-Cu dimers (see Fig. 16 and the Supplemental Material [7]) as well as for larger clusters with small finite size effects within the effective single-band Hubbard model. Then the estimated ratio $\rho_{\rm HK}$ of the FM on- and intersite contributions to $J_1$ reads [81]

$$\rho_{\rm HK} = \frac{J_1^{\rm H}}{J_1^{K_{pd}}} \approx \frac{J_1^H}{2K_{pd}[1 + (U_p - 2J_H)/\Delta_{pd})]} \left(\frac{t_{pd}}{\Delta_{pd}}\right)^2, \quad (20)$$

where an often used isotropic approximation defines $J_H$:

$$J_H = 0.5(U_p - U_{pp}). \quad (21)$$

In the case of ideal two-leg ladders, i.e., $\Phi = 90^\circ$ and $U_p = 4.4$ eV, Rice *et al.* [56] ignoring $K_{pd}$, derived a useful expression for the FM interladder coupling:

$$J_1^H = \frac{2t_{pd}^4}{\Delta_{pd}^2}\left[\frac{1}{E_T + 2\Delta_{pd}} - \frac{1}{E_S + 2\Delta_{pd}}\right], \quad (22)$$

where $E_T = 7.3$ eV ($E_S = 1.8$ eV) denote the energy of the Zhang-Rice triplet (singlet) state, respectively, for $t_{pd} = 1.3$ and $\Delta_{pd} = 3.3$ eV. Inserting these numbers into Eq. (22) one arrives at $J_1^H = 24.7$ meV and a frustation ratio of 6.7 using the experimental value $J_2 = J_{\rm leg} = 166$ meV. The QC result can be confirmed if the direct FM coupling and the residual AFM couplings from $\Phi \neq 90^\circ$ and that from the $dd$ channel are taken into account assuming equal leg and rung AFM exchange integrals. Experimentally, however, they differ slightly: $J_{\rm leg}/J_{\rm rung} \approx 1.1$ for $SrCu_2O_3$, which is caused by different O $2p$ onsite energies. We ignore this small difference $\sim$15 meV and use for the double-chain problem the experimental value of $J_{\rm leg} = J_2$. From Eq. (22) one estimates $-J_1^H \approx J_2/7 \approx 0.629$ eV. Using Eq. (22) one obtains 1/3 for the set in Ref. [15] and $\approx$1/4 for $K_{pd} \sim 100$ meV. Adopting nearly the same value for the ladder compound value as for LICO obtained here, one would arrive at $\alpha < 4$ to 5 in accord with a QC prediction for $SrCu_2O_3$ [83] (see also the Supplemental Material [7]). High-energy spectroscopy and more theoretical studies are desirable to put material specific upper limits on important $U_d$ and $J_H$. Without the $dd$ chanel, the INS data [9] were described at $J_H = 0.6$ eV by already enlarged values $K_{pd} = 81$ and 96 meV, in accord with our optical conductivity, EELS, and RIXS spectra for LICO [66,71,84,85]. Figures 15 and 16 clearly show the larger sensitivity of the singlet-triplet separation to $K_{pd}$ than to $J_H$, where only the triplet state is slightly affected. This confirms $K_{pd}$ as the key FM source.

To summarize, a precise general microscopic assignment of the origin of the observed large $J_1$-values is still difficult since $K_{pd}$, $J_H$, and the AFM $J_{dd}$ are involved. But without doubt $K_{pd}$ is the leading FM term. The short $d_{\rm Cu-Cu}$ leads to a sizable direct intersite AFM superexchange, negligible in corner-sharing cuprates with $\approx\sqrt{2}$ larger $d_{\rm Cu-Cu}$.

The FM $K_{pp}$ somewhat reduces the generic AFM $J_2$. Cuprates are usually classified as charge transfer insulators, which is not strictly valid here since the $J_1$ is certainly affected by the additional superexchange governed by the Cu $U_d$ and the hopping $t_{dd}$ [Eqs. (13)–(15)] as in standard Mott insulators.

Within a much simpler effective single-band extended Hubbard model, larger clusters can be treated exactly. Here we include, in addition to the NN transfer integral $t \equiv t_1$, the Hubbard onsite repulsion $U$, and a NNN counter part $t_2$ to the former, the NN and NNN intersite Coulomb interactions $V_1$ and $V_2$, respectively, two external exchange couplings $\tilde{J}_1$ (to allow for a FM NN exchange) and $\tilde{J}_2$ to account for the corresponding FM contribution to $J_2$ arising from $K_{pp}$ between O sites (see the Supplemental Material [7]). For a dimer, an exact analytical expression is available [86] beyond the Hubbard-model:

$$J_1 = \frac{\sqrt{16t^2 + \tilde{U}^2} - \tilde{U}}{2} + \tilde{J}_1, \quad (23)$$

where $\tilde{U} = U - V + \frac{3}{4}\tilde{J}_1$. For $U \gg |t|, |\tilde{J}_1|$ in Eq. (23) simplifies to [used in Eqs. (14) and (15) for the $dd$ channel]

$$J_1 \approx \frac{4t^2}{\tilde{U}} + \tilde{J}_1. \quad (24)$$

The second, "external," term on the right-hand side is FM, and it overcompensates the first one, which represents the non-negligible AFM superexchange. The dimer model provides also a direct tool for materials like $Li_3Cu_2SbO_6$, $Na_3Cu_2Sb(Te)O_6$, and other alternating FM-AFM chain compounds with a dominant FM NN exchange.

## VI. SUMMARY

A large magnon dispersion up to 53 meV was observed in CYCO. It is caused mainly by a large extracted FM NN coupling $J_{a1} = -24$ meV exceeding that for LICO [9] and represents the highest value detected so far for any FFESC cuprate. From our experience with CYCO, a successful search of the *full* dispersion, up to $\sim$45 meV would refine the $J_1$ and $J_2$ in LICO and Li(Na)$Cu_2O_2$. The NNN AFM $J_{a2} = 5.5$ meV puts CYCO near to criticality ($\alpha \sim 0.23$) for a 1D chain but not for strongly enough AFM coupled NN chains shifted by half a Cu-Cu distance. This chain structure causes an O mediated stable FM alignment of magnetic moments along the chain in a stacked structure of quasi-2D-Néel commensurate collinear magnetic ordering. From our analysis and microscopic arguments for systems with similar chains, we expect highly dispersive magnons for $La_6Ca_8Cu_{24}O_{41}$, $Ca_2Nd(Gd)_2Cu_5O_{10}$, and $SrCa_{13}Cu_{24}O_{41}$ including the slightly $h$-doped systems. Then the available magnon dispersion-law should be helpful.

Gaplike features are observed at $\sim$11.5 meV and $\sim$28 meV. The smaller gap at 11.5 meV is ascribed to phonon-magnon coupling while the gap at 28 meV is ascribed to quantum effects due to the AFM IC as well as to the non-negligible inhomogeneous cuprate chain structure caused by the misfit with the NN Ca/Y chains generic for the composite

symmetry of its two subsystems in CYCO and in the cases mentioned above. Both effects are most cooperative for a lock-in SS consisting of $Ca_2Y_2Cu_5O_{10}$ and $Ca_4Y_4Cu_{10}O_{20}$ domains.

The large $J_1$ values in CYCO and LICO provide deep insight into the microscopic exchange pointing to a dominant direct FM interaction $K_{pd} \sim 105$ meV, more important than the indirect O $2p_xp_y$ exchange mediated by the Hund's coupling $J_H$. Noteworthy, we found that the usually ignored direct Cu-Cu superexchange may somewhat reduce the effect of FM couplings. $J_H$ and $U_d$ should be studied systematically [68], especially in view of smaller empirical values of $J_H \leqslant 0.6$ eV reported for superoxides [67]. Although the issue of a large FM $J_1$ value is now almost unraveled, we are still left with a new question: given such natural $K_{pd} \sim 100$ meV, what is the reason for the markedly *lower* values for linarite and some FFESC materials? Presumably, ligand effects lowering the efficiency of $J_H$ and raising the O mediated superexchange.

Thus, seemingly well understood "classical" systems, studied already for many years, are still sources of surprises, deserved to be studied in more detail to elucidate the interactions behind the exchanges described by various spin-Hamiltonians and their interplay with structural details.

The Department of Energy will provide public access to these results of federally sponsored research in accordance with the DOE Public Access Plan [136].

## ACKNOWLEDGMENTS

This work has been partially supported by U.S. Department of Energy (DOE) Grant No. DE-FG02-13ER41967. ORNL is managed by UT-Battelle, LLC, under Contract No. DE-AC05-00OR22725 for the DOE. The United States Government retains, and the publisher, by accepting the article for publication, acknowledges that the United States Government retains a nonexclusive, paid-up, irrevocable, worldwide license to publish or reproduce the published form of this manuscript, or allow others to do so, for United States Government purposes. We used resources at the High Flux Isotope Reactor and Spallation Neutron Source, DOE Office of Science User Facilities, operated by the Oak Ridge National Laboratory. Support by the SFB 1143 of the Deutsche Forschungsgemeinschaft is acknowledged (S.N.). We thank U. Nitzsche for technical assistance and S. Johnston, D. Miloslavlevic, A. Tsirlin, O. Janson, J. Málek, R. Klingeler, W. E. A. Lorenz, T. Schmitt, C. Monney, J. van den Brink, U. Rößler, A. S. Moskvin, D. Khomskii, A. M. Oles, G. Sawatzky, K. Wohlfeld, A. Yaresko, S. Lebernegg, G. Roth, and J. Thar for discussions. Special thanks to G.R. and J.T. for providing figures of the $CuO_2$ chains in CYCO according to their structure model as well as to D.M., A.T., O.J., S.L., and U.N. for providing unpublished theoretical results included partly in Table I of the Supplemental Material [7]. We also thank J. Richter and A. Hauser for help with their HTE package code used here.

[1] R. Bursill, G. A. Gehring, D. J. J. Farnell, J. B. Parkinson, T. Xiang, and C. Zeng, J. Phys.: Condens. Matter **7**, 8605 (1995).

[2] M. Braden, G. Wilkendorf, J. Lorenzana, M. Aïn, G. J. McIntyre, M. Behruzi, G. Heger, G. Dhalenne, and A. Revcolevschi, Phys. Rev. B **54**, 1105 (1996).

[3] C. E. Agrapidis, S.-L. Drechsler, J. van den Brink, and S. Nishimoto, Phys. Rev. B **95**, 220404(R) (2017); SciPost Phys. **6**, 019 (2019).

[4] S.-L. Drechsler, O. Volkova, A. N. Vasiliev, N. Tristan, J. Richter, M. Schmitt, H. Rosner, J. Málek, R. Klingeler, A. A. Zvyagin, and B. Büchner, Phys. Rev. Lett. **98**, 077202 (2007).

[5] J. Sirker, Phys. Rev. B **81**, 014419 (2010).

[6] Y. Tarui, Y. Kobatashi, and M. Sato, J. Phys. Soc. Jpn. **77**, 043703 (2008).

[7] See Supplemental Material at http://link.aps.org/supplemental/10.1103/PhysRevB.100.104415 for additional information concerning the calculation of the dynamical structure factor and spin gaps for inhomogeneous chains (A), the microscopic theoretical description of the large $J_1$ - and $J_2$ -values (B,H), computational details of the employed quantum chemistry and density functional theory based calculations (C), the high-temperature expansion for the magnetic susceptibility, the Curie-Weiss temperature and the saturation field (F,G), and aspects of the criticality of the 2D magnetic structure (D) as well as of the phonon-mode probably responsible for the small gap near 11 meV (E), where A-H stand for the corresponding sections (See also Refs. [91–135]).

[8] J. Thar, R. Müller, S. Mattauch, B. Büchner, and G. Roth, Acta Cryst. **A62**, s185 (2006); see also J. Thar, Präparation und Charakterisierung von $(Ca_{1-x}Y_x)_4Cu_5O_{10} (0 < x < 0.5)$, Diplomerwork, Institut für Kristallografie, RWTH Aachen, Figs. 6.1, 6.7, 6.8, 6.10.

[9] W. E. A. Lorenz, R. O. Kuzian, S.-L. Drechsler, W.-D. Stein, N. Wizent, G. Behr, J. Málek, U. Nitzsche, H. Rosner, A. Hiess, W. Schmidt, R. Klingeler, M. Loewenhaupt, and B. Büchner, Europhys. Lett. **88**, 37002 (2009).

[10] W. E. A. Lorenz, On the spin-dynamics of the quasi-one-dimensional, frustrated quantum magnet $Li_2CuO_2$ studies by means of inelastic neutron scattering and thermodynamic methods, Ph.D. dissertation, TU Dresden, 2011, http://d-nb.info/1067190074/34.

[11] R. O. Kuzian, R. Klingeler, W. E. A. Lorenz, N. Wizent, S. Nishimoto, U. Nitzsche, H. Rosner, D. Milosavljevic, L. Hozoi, R. Yadav, J. Richter, A. Hauser, J. Geck, R. Hayn, V. Yushankhai, L. Siurakshina, C. Monney, T. Schmitt, J. Málek, G. Roth, J. Thar, T. Ito, H. Yamaguchi, M. Matsuda, S. Johnston, and S.-L. Drechsler, New J. Phys. **20**, 058001 (2018), in their late Corrigenda and the Reply by Shu *et al.*, *ibid.*, 059501 and 058002, respectively. Some incorrect statements still do remain to be discussed elsewhere [see also R. O. Kuzian *et al.*, arXiv:1708.06335v2 (2018)].

[12] M. Matsuda, K. Ohoyama, and M. Ohashi, J. Phys. Soc. Jpn. **68**, 269 (1999).

[13] H. F. Fong, B. Keimer, J. W. Lynn, A. Hayashi, and R. J. Cava, Phys. Rev. B **59**, 6873 (1999).

[14] V. Kargl, P. Böni, A. Mirmelstein, B. Roessli, and D. Sheptyakov, Physica B **359**, 1255 (2005).

[15] Y. Mizuno, T. Tohyama, S. Maekawa, T. Osafune, N. Motoyama, H. Eisaki, and S. Uchida, Phys. Rev. B **57**, 5326 (1998).

[16] M. S. Hybertsen, E. B. Stechel, M. Schluter, and D. R. Jennison, Phys. Rev. B **41**, 11068 (1990).

[17] M. S. Hybertsen, E. B. Stechel, W. M. C. Foulkes, and M. Schlüter, Phys. Rev. B **45**, 10032 (1992).

[18] V. S. Kargl, Magnetic properties of low dimensional spin systems, Ph.D. dissertation, TU Munich, 2006.

[19] P. K. Davies, E. Caignol, and T. King, J. Am. Ceram. Soc. **74**, 569 (1991).

[20] Due to the hybridization between the Cu $3d_{xz}$ and the bridging O $2p_z$ and $2p_x$ orbitals, the spin 1/2 is distributed between these three orbitals with a dominant Cu $3d$ weight $n_d \approx 0.78$ in accord with the observation of a finite O moment of $22 \pm 4\%$ [87]. Within the error bars the same ratio has been found earlier for the ordered moments also by neutron diffraction in the $CuO_2$ chains of $La_{14-x}Ca_xCuO_{24}O_{41}$ [88]. This ratio of the O and Cu occupation numbers is generic for FFES $CuO_2$ chain systems. In the formal limit $n_d \to 1$ CYCO and LICU would be *unfrustrated* AFM or FM simple quasi-1D pure Mott insulators with a weak AFM or FM NN exchange integral $J_{dd}$ of few meV and a weak magnon dispersion $\sim 2J_{dd}$.

[21] M. Matsuda, H. Yamaguchi, T. Ito, C. H. Lee, K. Oka, Y. Mizuno, T. Tohyama, S. Maekawa, and K. Kakurai, Phys. Rev. B **63**, 180403(R) (2001).

[22] M. Matsuda, K. Kakurai, M. Yethiraj, and K. Oka, J. Phys. Soc. Jpn. **74**, 1578 (2005).

[23] M. Matsuda, K. Kakurai, S. Kurogi, K. Kudo, Y. Koike, H. Yamaguchi, T. Ito, and K. Oka, Phys. Rev. B **71**, 104414 (2005).

[24] R. O. Kuzian, S. Nishimoto, S.-L. Drechsler, J. Málek, S. Johnston, J. van den Brink, M. Schmitt, H. Rosner, M. Matsuda, K. Oka, H. Yamaguchi, and T. Ito, Phys. Rev. Lett. **109**, 117207 (2012).

[25] B. Winn, U. Filges, V. Ovidiu Garlea, M. Graves-Brook, M. Hagen, C. Jiang, M. Kenzelmann, L. Passell, S. M. Shapiro, X. Tong, and I. Zaliznyak, EPJ Web of Conferences **83**, 03017 (2015).

[26] R. T. Azuah, L. R. Kneller, Y. Qiu, P. L. W. Tregenna-Piggott, C. M. Brown, J. R. D. Copley, and R. M. Dimeo, J. Res. Natl. Inst. Stand. Technol. **114**, 341 (2009).

[27] G. J. Shu, J. C. Tian, C. K. Lin, M. Hayashi, S. C. Liou *et al.*, New J. Phys. **19**, 023026 (2017).

[28] H. J. Xiang, C. Lee, and M. H. Whangbo, Phys. Rev. B **76**, 220411(R) (2007).

[29] S. Nishimoto, S.-L. Drechsler, R. O. Kuzian, J. van den Brink, J. Richter, W. E. A. Lorenz, Y. Skourski, R. Klingeler, and B. Büchner, Phys. Rev. Lett. **107**, 097201 (2011).

[30] S. Nishimoto, S.-L. Drechsler, R. Kuzian, J. Richter, and J. van den Brink, Phys. Rev. B **92**, 214415 (2015).

[31] S. You, Z. Li, L. Yang, C. Dong, L. Chen, C. Jin, J. Hu, G. Shen, and H. Mao, J. Solid State Chem. **182**, 3085 (2009).

[32] Z. Li, J. S. Tse, S. You, C. Q. Jin, and T. Litaka, J. Mod. Phys. B **25**, 3409 (2011).

[33] T. Schmitt and C. Monney (private communication, 2017).

[34] H. Yamaguchi, K. Oka, and T. Ito, Physica C **320**, 167 (1999).

[35] Y. Gotoh, I. Yamaguchi, S. Takeya, H. Fujihisa, K. Honda, T. Ito, K. Oka, and H. Yamaguchi, J. Alloys Compounds **408**, 1226 (2006).

[36] N. Wizent, Hochdruckkristallzüchtung von ausgewählten Oxiden, Ph.D. dissertation, TU Dresden, 2009.

[37] R. A. Cowley and G. Dolling, Phys. Rev. **167**, 464 (1968).

[38] R. Caciuffo, G. Amoretti, P. Santini, G. H. Lander, J. Kulda, and P. d. V. Du Plessis, Phys. Rev. B **59**, 13892 (1999).

[39] R. Caciuffo, P. Santini, S. Carretta, G. Amoretti, A. Hiess, N. Magnani, L.-P. Regnault, and G. H. Lander, Phys. Rev. B **84**, 104409 (2011).

[40] B. Rainford, J. Houmann, and H. Guggenheim, in *Neutron Inelastic Scattering 1972* (International Atomic Energy Agency, Vienna, 1972), p. 655.

[41] S. W. Lovesey, J. Phys. C **5**, 2769 (1972).

[42] M. Hennion and F. Moussa, New J. Phys. **7**, 84 (2005).

[43] R. J. McQueeney, M. Yethiraj, W. Montfrooij, J. S. Gardner, P. Metcalf, and J. M. Honig, Phys. Rev. B **73**, 174409 (2006).

[44] S. Johnston, C. Monney, V. Bisogni, K.-J. Zhou, R. Kraus, G. Behr, V. N. Strocov, J. Málek, S.-L. Drechsler, J. Geck, T. Schmitt, and J. van den Brink, Nat. Commun. **7**, 10563 (2016).

[45] W. S. Lee, S. Johnston, B. Moritz, J. Lee, M. Yi, K. J. Zhou, T. Schmitt, L. Patthey, V. Strocov, K. Kudo, Y. Koike, J. van den Brink, T. P. Devereaux, and Z. X. Shen, Phys. Rev. Lett. **110**, 265502 (2013).

[46] N. Wizent, N. Leps, G. Behr, R. Klingeler, B. Büchner, and W. Löser, J. Cryst. Growth **401**, 596 (2014).

[47] R. Fehrenbacher and T. M. Rice, Phys. Rev. Lett. **70**, 3471 (1993).

[48] E. Jeckelmann, Phys. Rev. B **66**, 045114 (2002).

[49] We mention formally the third scenario for $\delta > -J_1$. It reminds an alternating FM-AFM type case of weakly AFM coupled FM dimers, i.e., alternating pairs of $CuO_4$ units with $\Phi \approx \pi/2$ and big $\Phi \gtrsim 100^\circ$ with a sign change. Then the small gap is like that for a Haldane $S = 1$ chain with weak AFM coupling of spins 1 FM dimers with a large local gap, i.e., singlet excitations from triplet "ground states." Here we deal with *two* magnon branches and a smaller dispersion of each as that observed above. The opposite case with AFM dimers and weaker FM couplings has been recently proposed for $BaCu_2V_2O_8$ [7,89]. But it is unclear whether this model could describe also the observed smooth dispersion in a broad energy range up to 53 meV as shown clearly already by the two scenarios considered above. Hence, we regard the FM-AFM chain scenario as less likely relevant for CYCO than the other ones.

[50] K. Kudo, S. Kurogi, Y. Koike, T. Nishizaki, and N. Kobayashi, Phys. Rev. B **71**, 104413 (2005).

[51] A. Lohmann, H.-J. Schmidt, and J. Richter, Phys. Rev. B **89**, 014415 (2014).

[52] For the 10th-order HTE see the HTE10 package from http://www.uni-magdeburg.de/jschulen/HTE10/.

[53] S. Okubo, K. Kawakami, M. Yoshida, and H. Ohta, Phys. Status Solidi C **3**, 2828 (2006).

[54] S. A. Carter, B. Batlogg, R. J. Cava, J. J. Krajewski, W. F. Peck Jr., and T. M. Rice, Phys. Rev. Lett. **77**, 1378 (1996).

[55] M. Matsuda, K. Kakurai, J. E. Lorenzo, L. P. Regnault, A. Hiess, and G. Shirane, Phys. Rev. B **68**, 060406(R) (2003).

[56] T. M. Rice, B. Gopalan, and M. Sigrist, Europhys. Lett. **23**, 445 (1993).

[57] P. Müller, J. Richter, and D. Ihle, Phys. Rev. B **95**, 134407 (2017).

[58] M. Härtel, J. Richter, D. Ihle, and S.-L. Drechsler, Phys. Rev. B **78**, 174412 (2008).

[59] Y. Iqbal, P. Ghosh, R. Narayanan, B. Kumar, J. Reuther, and R. Thomale, Phys. Rev. B **94**, 224403 (2016).

[60] K. Caslin, R. K. Kremer, F. S. Razavi, A. Schulz, A. Muñoz, F. Pertlik, J. Liu, M.-H. Whangbo, and J. M. Law, Phys. Rev. B **89**, 014412 (2014).

[61] K. Caslin, R. K. Kremer, F. S. Razavi, M. Hanfland, K. Syassen, E. E. Gordon, and M.-H. Whangbo, Phys. Rev. B **93**, 022301 (2016).

[62] K. Caslin, Investigations of frustrated quasi–one-dimensional quantum spin-chain materials, Ph.D. dissertation, Brock University, St. Catharines, Ontario, Canada, 2015.

[63] A. Hayashi, B. Batlogg, and R. J. Cava, Phys. Rev. B **58**, 2678 (1998).

[64] F. Sapina, J. Rodriguez-Carvajal, M. Sanchis, R. Ibánez, A. Beltrán, and A. Beltrán, Solid State Commun. **74**, 779 (1990).

[65] J. Málek, S.-L. Drechsler, U. Nitzsche, H. Rosner, and H. Eschrig, Phys. Rev. B **78**, 060508(R) (2008).

[66] C. Monney, V. Bisogni, K.-J. Zhou, R. Kraus, V. N. Strocov, G. Behr, J. Málek, R. Kuzian, S.-L. Drechsler, S. Johnston, A. Revcolevschi, B. Büchner, H. M. Rønnow, J. van den Brink, J. Geck, and T. Schmitt, Phys. Rev. Lett. **110**, 087403 (2013).

[67] I. Solovyev, Z. Pchelkina, and V. Mazurenko, CrystEngCom **16**, 522 (2014).

[68] J. M. Tomczak (private communication); S.-L. Drechsler *et al.* (unpublished).

[69] In a recent RIXS-study for $Sr_{14}Cu_{24}O_{41}$ a significant related intersite Coulomb interaction $V_{pd} = 1.5$ eV had to be adopted [70] in accord with the theoretical recommendation for quasi-1D systems $V_{pd} \approx U_{dd}/5$ [90]. Similarly, to describe the optical conductivity and EELS data as well as the $J_1$ value for $Li_2CuO_2$, $V_{pd} = 0.95$ eV and $V_{dd} = V_{pp} = 0.2$ eV have been used [71,85].

[70] A. Higashiya, S. Imada, T. Murakawa, H. Fujiwara, S. Kasai, A. Sekiyama, S. Sugai, K. Okada, M. Yabashi, K. Tamasaku, T. Ishikawa, and H. Eisaki, New J. Phys. **10**, 053033 (2008).

[71] S.-L. Drechsler, J. Málek, R. Kuzian, S. Nishimoto, U. Nitzsche, W. Lorenz, R. Klingeler, B. Büchner, and M. Knupfer, Physica C **470**, S84 (2010).

[72] R. Neudert, H. Rosner, S.-L. Drechsler, M. Kielwein, M. Sing, Z. Hu, M. Knupfer, M. S. Golden, J. Fink, N. Nücker, M. Merz, S. Schuppler, N. Motoyama, H. Eisaki, S. Uchida, M. Domke, and G. Kaindl, Phys. Rev. B **60**, 13413 (1999).

[73] M. Schmitt, O. Janson, S. Golbs, M. Schmidt, W. Schnelle, J. Richter, and H. Rosner, Phys. Rev. B **89**, 174403 (2014).

[74] E. Bordas, C. de Graaf, R. Caballol, and C. J. Calzado, Phys. Rev. B **71**, 045108 (2005).

[75] C. J. Calzado, J. F. Sanz, and J. P. Malrieu, J. Chem. Phys. **112**, 5158 (2000).

[76] C. Koo, E. Zvereva, I. Zhukaev, M. Richter, M. Stratan, A. Vasiliev, V. Nalbandyan, and R. Klingeler, J. Phys. Soc. Jpn. **85**, 084702 (2016).

[77] Y. Miura, R. Hirai, Y. Kobayashi, and M. Sato, J. Phys. Soc. Jpn. **75**, 084702 (2006).

[78] Y. Miura, Y. Yasui, M. Moyoshi, M. Sato, and J. Kakurai, J. Phys. Soc. Jpn. **77**, 104709 (2008).

[79] Another relevant case is that of ferromagnetically coupled corner-sharing double (zigzag) chains as in $SrCuO_2$ and various ferromagnetically coupled ladder systems with a huge NNN AFM coupling $J_2 \gg -J_1$ which dominates their high-$T$ magnetic and dynamical response, hindering the extraction of $J_1$. An analysis of the FM $J_1$ value like that given here below has not yet been performed. The reported relatively large $J_1 \approx -30.8$ meV for $SrCu_2O_3$ was mainly caused in the simulations [15] by a more than three times smaller competing $J_\Phi$ via the bridging O as compared to LICU and CYCO [see Eq. (16)].

[80] S. Tornow, O. Entin-Wohlman, and A. Aharony, Phys. Rev. B **60**, 10206 (1999).

[81] W. Geertsma and D. Khomskii, Phys. Rev. B **54**, 3011 (1996).

[82] Notice the multiplication by a factor of $-2$ due to the different definitions of the spin Hamiltonians.

[83] E. Bordas, C. de Graaf, R. Cabasllol, and C. J. Colzado, Theor. Chim. Acc. **116**, 535 (2006).

[84] S.-L. Drechsler, J. Málek, W. E. A. Lorenz, R. O. Kuzian, R. Klingeler, S. Nishimoto, U. Nitzsche, M. Knupfer, N. Wizent, G. Behr, H. Rosner, H. Eschrig, and B. Büchner, J. Phys.: Conf. Ser. **200**, 012028 (2010).

[85] In cluster studies [44,65,66,71,84] within the five-band extended Hubbard model with up to six $CuO_4$ units, omitting $V_{dd}$ but with $V_{pd} = 0.95$ eV and an already enhanced $K_{pd} = 95$ meV, an enlarged $J_1$ value $\approx -19.8$ meV was obtained [see also Eq. (23)] within the effective single-band Hubbard-type model for $CuO_2$ plaquette.

[86] R. Schumann *et al.* (unpublished).

[87] M. Matsuda, K. Kakurai, H. Yamaguchi, T. Ito, C. Lee, and K. Oka, Appl. Phys. A **74**, s637 (2002).

[88] M. Matsuda, K. M. Kojima, Y. J. Uemura, J. L. Zarestky, K. Nakajima, K. Kakurai, T. Yokoo, S. M. Shapiro, and G. Shirane, Phys. Rev. B **57**, 11467 (1998).

[89] E. S. Klyushina, A. T. M. N. Islam, J. T. Park, E. A. Goremychkin, E. Wheeler, B. Klemke, and B. Lake, Phys. Rev. B **98**, 104413 (2018).

[90] K. Okada and A. Kotani, J. Phys. Soc. Jpn. **66**, 341 (1997).

[91] T. Helgaker, P. Jorgensen, and J. Oslen, *Molecular Electronic-Structure Theory* (Wiley, Chichester, 2000).

[92] N. B. Balabanov and K. A. Peterson, J. Chem. Phys. **123**, 064107 (2005).

[93] T. H. Dunning Jr., J. Chem. Phys. **90**, 1007 (1989).

[94] R. Dovesi, C. Ermondi, E. Ferrero, C. Pisani, and C. Roetti, Phys. Rev. B **29**, 3591 (1984).

[95] J. Sanz and J. Malrieu, J. Phys. Chem. **97**, 99 (1993).

[96] H.-J. Werner, P. J. Knowles *et al.*, Wiley Interdiscip. Rev.: Comput. Mol. Sci. **2**, 242 (2012).

[97] K. Koepernik and H. Eschrig, Phys. Rev. B **59**, 1743 (1999).

[98] I. Opahle, K. Koepernik, and H. Eschrig, Phys. Rev. B **60**, 14035 (1999).

[99] J. P. Perdew, K. Burke, and M. Ernzerhof, Phys. Rev. Lett. **77**, 3865 (1996).

[100] W. A. Harrison, *Electronic Structure and the Properties of Solids* (Freeman, San Francisco, 1980).

[101] M. Matsuda, K. Katsumata, T. Yokoo, S. M. Shapiro, and G. Shirane, Phys. Rev. B **54**, R15626(R) (1996).

[102] F. Heidrich-Meisner, A. Honecker, and T. Vekua, Phys. Rev. B **74**, 020403(R) (2006).
[103] H. T. Lu, Y. J. Wang, S. Qin, and T. Xiang, Phys. Rev. B **74**, 134425 (2006).
[104] H.-J. Schmidt, A. Lohmann, and J. Richter, Phys. Rev. B **84**, 104443 (2011).
[105] H.-J. Schmidt, J. Schnack, and M. Luban, Phys. Rev. B **64**, 224415 (2001).
[106] S. E. Dutton, M. Kumar, M. Mourigal, Z. S. Soos, J.-J. Wen, C. L. Broholm, N. H. Andersen, Q. Huang, M. Zbiri, R. Toft-Petersen, and R. J. Cava, Phys. Rev. Lett. **108**, 187206 (2012).
[107] M. Bosiočic, F. Bert, S. E. Dutton, R. J. Cava, P. J. Baker, M. Požek, and P. Mendels, Phys. Rev. B **96**, 224424 (2017).
[108] H.-J. Grafe, S. Nishimoto, M. Jakovleva, E. Vavilova, L. Spillecke, A. Alfonsov, M.-I. Sturza, S. Wurmehl, H. Nojiri, H. Rosner, J. Richter, U. K. Rößler, S.-L. Drechsler, V. Kataev, and B. Büchner, Sci. Rep. **7**, 6720 (2017).
[109] K. Nawa, Y. Okamoto, A. Matsuo, K. Kindo, Y. Kitahara, S. Yoshida, S. Ikeda, S. Hara, T. Sakurai, S. Okubo, H. Ohta, and Z. Hiroi, J. Phys. Soc. Jpn. **83**, 103702 (2014).
[110] O. Janson, A. A. Tsirlin, M. Schmitt, and H. Rosner, Phys. Rev. B **82**, 014424 (2010).
[111] H. Rosner, Electronic structure and exchange integrals of low-dimensional cuprates, Ph.D. dissertation, TU Dresden, 1999.
[112] Y. J. Kim, R. J. Birgeneau, F. C. Chou, M. Greven, M. A. Kastner, Y. S. Lee, B. O. Wells, A. Aharony, O. Entin-Wohlman, I. Ya. Korenblit, A. B. Harris, R. W. Erwin, and G. Shirane, Phys. Rev. B **64**, 024435 (2001).
[113] P. Babkevich, N. E. Shaik, D. Lançon, A. Kikkawa, M. Enderle, R. A. Ewings, H. C. Walker, D. T. Adroja, P. Manuel, D. D. Khalyavin, Y. Taguchi, Y. Tokura, M. Soda, T. Masuda, and H. M. Rønnow, Phys. Rev. B **96**, 014410 (2017).
[114] S. Fatale, C. G. Fatuzzo, P. Babkevich, N. E. Shaik, J. Pelliciari, X. Lu, D. E. McNally, T. Schmitt, A. Kikkawa, Y. Taguchi, Y. Tokura, B. Normand, H. M. Rønnow, and M. Grioni, Phys. Rev. B **96**, 115149 (2017).
[115] A. N. Yaresko, A. Y. Perlov, R. Hayn, and H. Rosner, Phys. Rev. B **65**, 115111 (2002).
[116] V. Y. Yushankhai and R. Hayn, Europhys. Lett. **47**, 116 (1999).
[117] M. Schmitt, Microscopic description of magnetic model compounds, Ph.D. dissertation, TU Dresden, 2011.
[118] Y. Yasui, N. Igawa, and K. Kakurai, JPS Conf. Proc. **8**, 034012 (2015).
[119] S. Nishimoto, S.-L. Drechsler, R. O. Kuzian, J. Richter, J. Málek, M. Schmitt, J. van den Brink, and H. Rosner, Europhys. Lett. **98**, 37007 (2012).
[120] S. J. Hibble, J. Köhler, A. Simon, and S. Paiser, J. Solid State Chem. **88**, 534 (1990).
[121] A. A. Gippius, E. N. Morozova, A. S. Moskvin, A. V. Zalessky, A. A. Bush, M. Baenitz, H. Rosner, and S.-L. Drechsler, Phys. Rev. B **70**, 020406(R) (2004).
[122] L. Capogna, M. Reehuis, A. Maljuk, R. K. Kremer, B. Ouladdiaf, M. Jansen, and B. Keimer, Phys. Rev. B **82**, 014407 (2010).
[123] M. Schäpers, H. Rosner, S.-L. Drechsler, S. Süllow, R. Vogel, B. Büchner, and A. U. B. Wolter, Phys. Rev. B **90**, 224417 (2014).
[124] K. C. Rule, B. Willenberg, M. Schäpers, A. U. B. Wolter, B. Büchner, S.-L. Drechsler, G. Ehlers, D. A. Tennant, R. A. Mole, J. S. Gardner, S. Süllow, and S. Nishimoto, Phys. Rev. B **95**, 024430 (2017).
[125] I. A. Zaliznyak, H. Woo, T. G. Perring, C. L. Broholm, C. D. Frost, and H. Takagi, Phys. Rev. Lett. **93**, 087202 (2004).
[126] K. Sparta, A. Löffer, C. Gross, W. Aßmus, and G. Roth, Z. Kristallogr. **221**, 782 (2006).
[127] K. Ruck, M. Wolf, M. Ruck, D. Eckert, G. Krabbes, and K. H. Müller, Mat. Res. Bull. **36**, 1995 (2001).
[128] V. Bisogni, S. Kourtis, C. Monney, K. Zhou, R. Kraus, C. Sekar, V. Strocov, B. Büchner, J. van den Brink, L. Braicovich, T. Schmitt, M. Daghofer, and J. Geck, Phys. Rev. Lett. **112**, 147401 (2014).
[129] G. Deng, D. Yu, R. Mole, E. Pomjakushina, K. Conder, M. Kenzelmann, S.-i Yano, C.-W. Wang, K. C. Rule, J. S. Gardner, H. Luo, S. Li, C. Ulrich, P. Imperia, W. Ren, S. Cao, and G. J. McIntyre, Phys. Rev. B **98**, 184411 (2018).
[130] S. Lebernegg, A. A. Tsirlin, O. Janson, and H. Rosner, Phys. Rev. B **88**, 224406 (2013).
[131] J. Holmlund, C. S. Knee, J. Andreasson, M. Granath, A. P. Litvinchuk, and L. Börjesson, Phys. Rev. B **79**, 085109 (2009).
[132] J. P. Perdew and Y. Wang, Phys. Rev. B **45**, 13244 (1992).
[133] L. Balents and O. A. Starykh, Phys. Rev. Lett. **116**, 177201 (2016).
[134] J. Sudan, A. Lüscher, and A. M. Läuchli, Phys. Rev. B **80**, 140402(R) (2009).
[135] S.-L. Drechsler, J. Richter, R. Kuzian, J. Málek, N. Tristan, B. Büchner, A. S. Moskvin, A. A. Gippius, A. Vasiliev, O. Volkova, A. Prokofiev, H. Rakoto, J.-M. Broto, W. Schnelle, M. Schmitt. A. Ormeci, C. Loison, and H. Rosner, J. Magn. Magn. Mater. **316**, 306 (2007).
[136] http://energy.gov/downloads/doe-public-access-plan.